https://doi.org/10.5194/egusphere-2024-4088
Preprint. Discussion started: 21 January 2025

A dynamical separation of deep and shallow branches in the stratospheric circulation

Rasul Baikhadzhaev[1], Felix Ploeger[1,2], Peter Preusse[1], Manfred Ern[1], and Thomas Birner[3]

[1]Institute of Climate and Energy Systems: Stratosphere (ICE-4), Forschungszentrum Jülich, Jülich, Germany.
[2]Institute for Atmospheric and Environmental Research, University of Wuppertal, Wuppertal, Germany.
[3]Meteorological Institute Munich, Ludwig Maximilians University of Munich, Munich, Germany.

Correspondence: Rasul Baikhadzhaev (r.baikhadzhaev@fz-juelich.de)

Abstract. The wave driven Brewer-Dobson circulation plays a crucial role in determining the transport of trace gases and aerosols in stratosphere. We examine the structure of the circulation based on reanalyses data (ERA5, ERA-Interim, MERRA2, JRA55), using the Transformed Eulerian Mean and downward control framework, aiming for a dynamical separation of different circulation branches in terms of outflow generated by wave driving. The results show the existence of different circulation regimes, with a deep circulation branch mainly driven by large-scale waves with wavenumbers 1-3, and a shallow circulation branch mainly driven by smaller-scale waves with wavenumbers 4-180. We propose a definition of the separation level between a shallow and deep branch as the lowest level where outflow from waves 1-3 is larger than from waves 4-180. We show that this level occurs at approximately 22km (43hPa) and exhibits a weak annual cycle. This climatological structure is robust in various reanalyses. The variability of the circulation in the deep branch above the separation level is mainly related to large-scale waves 1-3, while the variability in the shallow branch is related to both smaller-scale and large-scale waves. Trends in the circulation over the period 1980-2017 show an upward shift of the deep branch related to waves 1-3 and a downward shift of the shallow branch related to both large and smaller scale waves. The height of the separation level shows no significant trend. Taking into account differences in wave driving between the branches of the circulation could reduce the spread in model inter-comparisons.

1 Introduction

The global stratospheric circulation, also termed the Brewer–Dobson circulation (BDC), plays a crucial role in the climate system as it shapes the distributions of chemical and radiatively active species in the upper troposphere and lower stratosphere (UTLS). Particularly in the UTLS region, small changes in radiatively active species, like water vapour and ozone, can cause substantial radiative effects (e.g. Solomon et al., 2010; Riese et al., 2012) and impacts on atmospheric circulation (Charlesworth et al., 2023).

The BDC is characterized by upward transport of air masses in the tropical stratosphere, poleward transport in the stratosphere, and downward transport at middle and high latitudes (Holton et al., 1995; Butchart, 2014). As a mechanically–forced circulation, the BDC is driven by atmospheric waves travelling upwards from the troposphere. These waves break higher up in the stratosphere and deposit their momentum to the background flow. This mechanism drives poleward mass flow in the subtropical

https://doi.org/10.5194/egusphere-2024-4088
Preprint. Discussion started: 21 January 2025

and middle latitude stratosphere, upwelling in the tropics and downwelling at high latitudes, and hence the global-scale Brewer-Dobson circulation in the meridional plane. It is a zoo of different waves which drive the stratospheric circulation at different levels, including planetary-scale, synoptic-scale and small-scale gravity waves (e.g. Plumb, 2002). The structure of the background flow in the stratosphere determines where the different waves break, deposit their momentum, and finally cause the forcing of the circulation (Andrews et al., 1987).

From a zonal mean perspective, transport by the BDC can be separated into a residual mean mass circulation and additional, two-way eddy mixing without any net mass transport. Still, the two-way eddy mixing may cause transport of trace gases, due to the strong gradients of these gases in the stratosphere. The residual circulation velocities can be directly related to the wave forcing using the Transformed Eulerian Mean (TEM) framework (Andrews et al., 1987). As found by Haynes et al. (1991), the upward mass flow in the tropics is caused by the wave forcing from all atmospheric levels above ("Downward Control" principle). Hence, variations in tropical upward mass flow across a given level ("tropical upwelling") are expected to correlate with variations in the wave drag above that level.

A closer look at the detailed structure of the stratospheric circulation reveals different circulation branches (Plumb, 2002), comprising a shallow circulation branch in the lower stratosphere, and a deep circulation branch extending to high altitudes and latitudes (Birner and Bönisch, 2011). Birner and Bönisch (2011) found a clear distinction of these two circulation branches in terms of transit times along the residual circulation and minimum pressure reached by the air parcels travelling with the residual circulation flow. Based on their trajectory analysis, the shallow circulation branch extends throughout the subtropics and mid-latitudes, vertically up to about 30–50 hPa. Motivated by these results, Lin et al. (2013) defined the shallow circulation branch to extend up to 30 hPa, the deep branch to be located above that level, and an additional transition branch in the lowest stratosphere below 70 hPa. These simplified definitions have the advantage that they equally divide the tropical upward mass flux between the shallow and deep branches, and have been applied for multi-model inter-comparisons of the BDC strength and changes therein (Lin et al., 2013). Furthermore, the shallow and deep stratospheric circulation branches have been argued to be driven by different mechanisms. Gerber (2012) showed from simulations with a mechanistic model that the shallow branch is mainly "tropospherically controlled" by variations of wave sources close to the surface, whereas the deep branch is "stratospherically controlled" by the structure of the stratospheric wave guide.

In a future climate, the stratospheric circulation is expected to increase as a response to increasing carbon dioxide levels, and climate models simulate this increase very robustly and throughout the stratosphere (e.g. Butchart, 2014). As the stratospheric residual circulation is too slow to be directly measurable, its strength needs to be inferred indirectly from observations. One commonly used diagnostic for that is stratospheric mean age of air, i.e. the average transit time of air parcels through the stratosphere (Waugh and Hall, 2002). In the lower stratosphere, most recent inter-comparisons show decreasing stratospheric mean age of air, indicating a circulation increase over time also in observation-based datasets, and hence consistency with climate model simulations (Garny et al., 2024). At upper levels in the middle stratosphere, there is a remaining discrepancy between stratospheric circulation trends simulated by free-running climate models and observation-based estimates (Garny et al., 2024), which had been already noted for different generations of climate models (e.g. Abalos et al., 2021; Butchart, 2014; Waugh, 2009). At these upper levels, climate models generally simulate an increasing circulation while in-situ and

https://doi.org/10.5194/egusphere-2024-4088
Preprint. Discussion started: 21 January 2025

satellite observations show increasing age of air (Ray et al., 2014; Mahieu et al., 2014; Stiller et al., 2017), but with related uncertainties being too large to disprove model predictions (Garny et al., 2024).

Meteorological reanalyses combine model simulations with observational data by data assimilation, and investigations of the stratospheric circulation in these datasets can give additional insights. In the lower stratosphere, most recent reanalyses show decreasing mean age while in the middle stratosphere mean age trends may differ even in sign between different reanalyses (Chabrillat et al., 2018; Ploeger et al., 2019). On the other hand, residual circulation trends in meteorological reanalysis datasets have been shown to have larger spread in the lower stratosphere and a more robust circulation increase emerges at upper levels above about 20 km (Abalos et al., 2015). Such differences between trends in residual circulation and trends in age of air are likely related to the fact that age of air is not solely controlled by the residual circulation but also strongly affected by mixing processes (Waugh and Hall, 2002). Overall, differences in the vertical structure of stratospheric circulation trends between different datasets raise the question as to whether the dynamical processes driving these changes also differ vertically.

Analysis of the forcing of circulation trends in climate models at a given level shows that particularly the partitioning into contributions of different wave types differs substantially between different models (Abalos et al., 2021). These discrepancies in circulation and wave forcing trends might potentially be attributed to variations in the depths of circulation branches across different datasets, such that comparisons at a given level might contrast different dynamical regimes. Hence, an improved interpretation of the stratospheric circulation and its potential changes requires an improved and more detailed understanding how the different (shallow and deep) circulation branches are separated dynamically.

In this paper, we investigate the stratospheric residual mean mass circulation and its wave forcing and aim for a dynamical separation criterion for different circulation branches. The analysis involves circulation estimates based on the TEM framework and on the downward control principle, as well as separation into contributions from different waves. These diagnostics are applied to various meteorological reanalyses. Specific research questions raised for this paper are: (i) Can different branches in the stratospheric circulation be dynamically defined based on the wave driving? (ii) Did different branches of the stratospheric circulation change differently over the past decades? (iii) How robust is the representation of the circulation structure and its changes in different reanalyses?

The applied circulation diagnostics and considered reanalysis data are described in Sect. 2. Thereafter, Sect. 3 investigates the climatological structure of the stratospheric circulation. Section 4 further focusses on variability and trends in the stratospheric circulation. The results are discussed in the context of existing literature in Sect. 5 before presenting the final conclusions of the paper.

2 Data and methods

2.1 Reanalysis data

Reanalyses aim to produce time-consistent datasets by integrating available observations through data assimilation to a 'fixed' version of Numerical Weather Prediction (NWP) model, thus providing the most complete data on past climate. The NWP model, its version, set of incorporated observations, and data assimilation methods depend on the assimilation center and on

https://doi.org/10.5194/egusphere-2024-4088
Preprint. Discussion started: 21 January 2025

the version of the analysis. In this work we use data from four global reanalyses: the Modern-Era Retrospective analysis for Research and Applications, Version 2 (MERRA-2) from the National Aeronautics and Space Administration (NASA) (Gelaro et al., 2017), the Japanese 55-year Reanalysis (JRA55) from the Japan Meteorological Agency (JMA) (Kobayashi et al., 2015), the ERA-Interim (Dee et al., 2011) and ERA5 (Hersbach et al., 2020) reanalyses from the European Centre for Medium-Range Weather Forecasts (ECMWF). The main focus is on ERA-5 which is the most recent reanalysis among these four and its enhanced horizontal and vertical resolution is expected to result in improved ability to resolve smaller-scale waves. Other reanalyses are mostly used for comparison and uncertainty estimation. In order to preserve consistency while performing inter-comparison, data from all used reanalyses were truncated to a common period of availability from 1980 to 2017. In order to save storage space, computational time, and for simpler inter-comparison, data from the reanalyses was resampled to 1° by 1° horizontal grid, interpolated to ERA5 vertical levels, and the temporal sampling was reduced to 6 hours. The effect of the resampling on ERA5 data is further explored in Sect. 5.

Figure 1 is based on ERA5 data. The residual circulation is shown in the left part of the figure as purple arrows with white contours. The two branches of the overturning circulation are clearly visible in the figure - the deep branch transfers mass from the tropical tropopause to the middle and upper stratosphere and towards the winter pole, and the shallow branch acting in the lower part of the stratosphere creates a mass flux from the tropics towards both poles.

2.2 Residual circulation diagnosis

In this paper we apply the Transformed Eulerian Mean (TEM) framework (Andrews et al., 1987) to diagnose and investigate the residual mean mass circulation. The vertical and horizontal components of the residual circulation in log-pressure coordinates are hence defined through

$$\begin{aligned} \bar{v}^* &= \bar{v} - \rho_0^{-1}(\rho_0 \overline{v'\theta'}/\bar{\theta}_z)_z \\ \bar{w}^* &= \bar{w} + (a\,cos(\phi))^{-1}(cos(\phi)\,\overline{v'\theta'}/\bar{\theta}_z)_\phi \end{aligned} \tag{1}$$

where an overbar represents zonal mean, a prime is the deviation from the mean, subscripts denote partial derivative, v is meridional velocity, ρ_0 is basic density, θ is potential temperature, w is vertical velocity, and a is mean radius of the Earth.

Energy deposition from wave breaking is the driver of the residual circulation. The wave breaking results in eddy potential vorticity flux which constitutes the Eliassen-Palm flux (EP flux). The divergence of the EP flux is generally used to determine wave drag and its driving of the stratospheric residual circulation. Latitudinal and vertical components of EP flux are defined by

$$\begin{aligned} F^{(\phi)} &= \rho_0 a\,cos(\phi)\,(\bar{u}_z \overline{v'\theta'}/\bar{\theta}_z - \overline{v'u'}) \\ F^{(z)} &= \rho_0 a\,cos(\phi)\{[f - (a\,cos(\phi))^{-1}(\bar{u}\,cos(\phi))_\phi]\overline{v'\theta'}/\bar{\theta}_z - \overline{w'u'}\} \end{aligned} \tag{2}$$

where u is zonal wind velocity, f is the Coriolis parameter defined as $2\Omega\,sin(\phi)$, where Ω is the angular velocity of the Earth.

https://doi.org/10.5194/egusphere-2024-4088
Preprint. Discussion started: 21 January 2025

The divergence of the EP-flux constitutes the driving force in the zonal momentum balance equation due to breaking atmospheric waves

$$\frac{\partial \bar{u}}{\partial t} + \bar{v}^*\left(\frac{1}{a\,cos(\phi)v}\frac{\partial \bar{u}\,cos(\phi)}{\partial \phi} - f\right) + \bar{w}^*\frac{\partial \bar{u}}{\partial z} = \frac{\nabla \cdot F}{\rho_0 a cos\phi} + \bar{X} \tag{3}$$

where X includes contributions from parameterized wave drag and will not be further considered in this paper which focuses on the contribution from resolved waves.

Individual wave contribution to the EP flux can be estimated by Fourier transformation of the three-dimensional EP flux data from longitude to wavenumber-frequency domain. The thus transformed components of the EP flux are defined through

$$\begin{aligned} F^{(\phi)}(s) &= \rho_0 a\,cos(\phi) Re[\bar{u_z}\hat{v}(s)\hat{\theta}^*(s)/\bar{\theta_z} - \hat{u}(s)\hat{v}^*(s)] \\ F^{(z)}(s) &= \rho_0 a\,cos(\phi) Re\{[f - (a\,cos(\phi))^{-1}(\bar{u}\,cos(\phi))_\phi]\hat{v}(s)\hat{\theta}^*(s)/\bar{\theta_z} - \hat{u}(s)\hat{w}^*(s)\} \end{aligned} \tag{4}$$

where Re denotes real part of a complex number, asterisk denotes complex conjugates, hat represents Fourier coefficient and s is the wavenumber index.

Here, wavenumber represents the spatial scale of the wave, the number of waves per 360 degrees of longitude, with wavenumber 1 (hereafter referred to as wave 1) being the largest possible wave. In this work the reanalysis data has been resampled to a 1 by 1 degree horizontal grid, and the Nyquist criterion requirement is at least 2 data points per wave. As a result, wave 180 is the shortest wave resolved in this study.

The wave dissipation given by the divergence of the EP flux and the residual circulation are connected through the downward control principle (DWCP)(e.g. Haynes et al., 1991). The DWCP states that the mass flow across a given level is related to just the momentum deposition from dissipating waves above that level. We use this relation to estimate the relative contribution of different waves to the driving of the residual circulation. Based on the DWCP, the following expressions can be derived for the residual mass stream function $\bar{\psi}^*_D$ and for the components of the residual circulation $\bar{v}^*_D, \bar{w}^*_D$

$$\bar{\psi}^*_D = \int_z^\infty \frac{a\,cos(\phi)\nabla \cdot F}{[a\,cos(\phi)(\bar{u} + a\,cos(\phi)\,\Omega)]_\phi}\,dz \tag{5a}$$

$$\bar{v}^*_D = \frac{1}{\rho_0\,cos(\phi)}\frac{\partial \bar{\psi}^*_D}{\partial z} \tag{5b}$$

$$\bar{w}^*_D = \frac{1}{a\rho_0\,cos(\phi)}\frac{\partial \bar{\psi}^*_D}{\partial \phi} \tag{5c}$$

The integration in Eq. 5a should actually be performed on constant angular momentum isolines. However, since outside the tropics the latitude and angular momentum isolines are close to parallel, we perform the integration on constant latitudes (cf. Abalos et al., 2015) and estimate the mean residual circulation upwelling between 20°S and 20°N by integration of Eq. 5c.

$$\bar{w}^{*\bar{\phi\pm}}_D = \frac{\bar{\psi}^{*\phi-}_D - \bar{\psi}^{*\phi+}_D}{a\rho_0 S^{\phi\pm}} \tag{6}$$

where S is area, $^{\phi-}$ is at southern latitude, $^{\phi+}$ is at northern latitude, $^{*\bar{\phi\pm}}$ denotes mean value between $\phi+$ and $\phi-$, and $^{*\phi\pm}$ denotes total between the latitudes.

https://doi.org/10.5194/egusphere-2024-4088
Preprint. Discussion started: 21 January 2025

The turn-around latitudes (TAL) separate the area of upward residual velocity in the tropical stratosphere from the area of downward velocity in the extratropics (eg. (Abalos et al., 2015)). In this work, tropical upwelling is defined as the total mass flow between the TAL carried by $\bar{w}^*$, and tropical outflow is defined as the poleward mass flow across TAL. The outflow at a given level represents the result of "gyroscopic pumping", indicating the amount of air mass being pulled from the tropics to middle and high latitudes by the wave drag at that level. The tropical upwelling, on the other hand, represents the integrated effect of the wave drag at all levels above, as described by the downward control principle (see above). Hence, with the tropical upwelling given by

$$W = 2\pi a^2 \rho_0 \int_{\phi_-}^{\phi_+} \bar{w}^* \, cos(\phi) d\phi \,, \tag{7}$$

the outflow out of the tropics at a given level is the top to bottom vertical derivative of the upwelling

$$V = -\frac{\partial W}{\partial z} \,. \tag{8}$$

There are two major wave types which drive the overturning circulation, Rossby and gravity waves. Planetary and synoptic scale Rossby waves are large-scale and driven by horizontal gradient of potential vorticity, these waves are influenced by the Earth's rotation, the latitudinal gradient of Coriolis parameter, and the mean zonal flow. The gravity waves are smaller-scale, less dependant on the Earth's rotation and primarily result from the interaction between buoyancy and inertia. The upward propagation of Rossby waves is controlled by the Charney-Drazin condition(Vallis, 2006), which for stationary waves is

$$0 < \bar{u} < \frac{f_\phi}{k^2 + l^2 + (f_0/2NH)^2} \tag{9}$$

where k and l are zonal and meridional wavenumbers, f_0 is a reference value of the Coriolis parameter, and N is the buoyancy frequency. This condition implies that Rossby waves may propagate upwards into the stratosphere if the zonal flow is eastward and weaker than a critical value. This critical value is higher for larger-scale waves (smaller k, l) such that these waves may propagate deeper into the stratosphere compared to smaller-scale waves.

3 Climatological structure of the stratospheric circulation

Figure 1 shows the climatology of the residual mean mass circulation of the BDC for the period 1980-2017 together with the resolved wave drag quantified in terms of the Eliassen-Palm flux divergence, which constitutes the circulation's driving force (see Eq. 4). Note that the EP flux divergence $\nabla \cdot F$ has been scaled by $\Delta t(a\rho_0 \, cos\phi)^{-1}$, with $\Delta t = 86400$s, to obtain the wave drag in $\mathrm{m\,s^{-1}\,day^{-1}}$. The expected features of the BDC, with tropical upwelling, poleward motion and extra-tropical downwelling and a stronger circulation cell in the winter hemisphere, are all evident in Fig. 1 (with colors representing resolved wave dissipation, "wave drag" in the following).

The reduced wave drag in the middle and upper stratosphere in the summer hemisphere is due to the presence of westward winds which prohibit Rossby waves to propagate upwards, known as the Charney-Drazin criterion (Charney and Drazin, 1961).

https://doi.org/10.5194/egusphere-2024-4088
Preprint. Discussion started: 21 January 2025

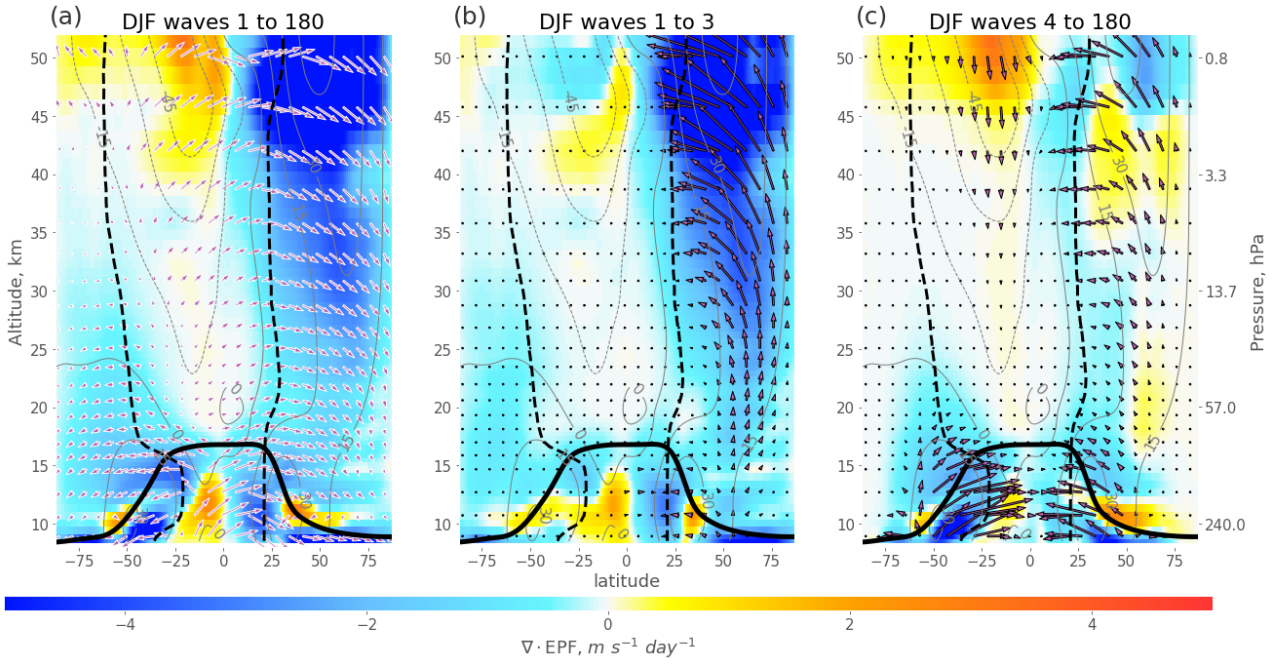

Figure 1. Climatalogical (1980-2017) distributions of resolved wave drag (estimated as Eliassen–Palm flux divergence, color coded) together with Eliassen–Palm flux vectors (black contour arrows), log scaled TEM residual circulation (white contour arrows), zonal mean zonal wind (grey contours) from ERA5 reanalysis for December–February. The distributions are shown for the contribution from all resolved waves (left), from large-scale waves with wavenumbers 1–3 (middle) and from smaller-scale waves with wavenumbers 4–180 (right). The black dashed lines show the turn-around latitudes (where upwelling in tropics changes to downwelling in extratropics), the thick black line shows the tropopause.

The wave filtering resulting from this criterion prevents the propagation of waves through a medium with an eastward wind speed above a certain threshold or any westward wind see eq. 9. The wind threshold depends on the wavenumber and is inversely proportional to it. Therefore, as shown in the second and third columns of the figure, large-scale Rossby waves are more likely to meet the criterion and are generally allowed to propagate deeper into the stratosphere. As a result, the majority of small-scale Rossby waves with wavenumbers larger than 3 break in the lower part of the stratosphere. The gravity waves are able to propagate deeper into the atmosphere and drive the mesospheric circulation. The seasonality of the BDC causes seasonal movement of the TAL with significant displacement into the summer hemisphere (Fig 1, dashed black lines).

The most important for driving the tropical upwelling into the stratosphere is the wave drag in close proximity to TAL as it is ultimately responsible for the uplift in the tropics (Eluszkiewicz et al., 2000).

The northern TAL in the lower part of the stratosphere is usually located between 20 to 40 degrees north of the equator. Figure 2 displays the time series of the wave drag and horizontal component of residual circulation estimated using the TEM

https://doi.org/10.5194/egusphere-2024-4088
Preprint. Discussion started: 21 January 2025

approach and DWCP at 70 hPa between 20 and 40 degrees north. The close relation between horizontal velocity vBarStar and wave drag is illustrated in the figure. Overall, the net outflow velocity calculated using TEM approach agrees well with the outflow calculated from all resolved waves and their variability correlates well with net resolved wave drag estimated from divergence of EP flux. The difference in residual circulation velocity between the TEM approach (green dashed line in Fig. 2) and the Downward Control principle (black dashed line) at 70 hPa appears to be due to the fact that the DWCP Eq. 5a only accounts for resolved wave drag while the full horizontal velocity based on the TEM definition is affected also by small-scale parameterized gravity waves. As a result, the residual circulation generated by waves 1 to 180 is weaker than the one obtained taking into account the total wave drag including parameterizations, using the TEM approach. This deficit is shown in Fig. A2 and discussed in more detail in Sect. 5.

As might be expected, the wave drag at the considered level $\nabla \cdot EPF$ (solid lines in Fig. 2), and the horizontal component of the residual circulation estimated from the wave drag above using the DWCP $\bar{v}^*_D$ (dashed lines in the figure) are consistent and have similar variability. The wave driving at 70 hPa in the Fig. 2 shows that about 3/4 of the circulation at the level is being driven by waves smaller than wave 3. However despite driving only 1/4 of the circulation, the large-scale waves 1 to 3 influence the variability of the circulation almost as much as the smaller-scale waves. Wave driving behind variability of the circulation is discussed in more details in Sect. 4.

The wave filtering due to the Charney-Drazin criterion related to the pattern of zonal wind (Fig. 1) limits the propagation of smaller-scale Rossby waves into the middle and upper stratosphere. As a result, the smaller-scale waves that do reach the stratosphere are expected to break and deposit their momentum at lower levels. Thus smaller-scale waves are expected to drive the shallow branch and large-scale planetary waves to drive the deep branch of the residual circulation (Plumb, 2002).

We analyze more precisely which waves are driving the deep and shallow circulation branches by applying both a mechanistic and a statistical method. In the statistical method we consider the correlation at the TAL between the outflow velocity defined as (negtive for northern hemisphere and positive for southern) horizontal component of the residual circulation estimated using the TEM formulation ($\bar{v}^*$) and the divergence of the Eliassen-Palm flux representing different wave bands $\nabla \cdot EPF$. The correlation coefficient between EPF divergence derived from total resolved wave drag and outflow velocity is close to 0.8 - 0.9 with exception of area below 20km where the correlation is somewhat weaker. For the wave driving separation of the deep and shallow branch we use difference between the largest waves drag correlation with outflow velocity and smaller-scale waves drag correlation with outflow velocity. Having vertical profiles of these differences (Fig. 3a, b), where negative coefficient means that drag of smaller scale waves has better correlation with EPF divergence, and positive coefficient means the largest waves drag correlates better. For the largest waves drag the correlation with the outflow velocity is high at upper levels but significantly weakens at levels below about 23km in both hemispheres. For the smaller-scale waves drag the correlation is high at the lower levels around 20km and weakens somewhat at higher levels. The mechanistic approach using the DWCP shows a similar separation between different waves in driving the circulation at different levels. Large-scale planetary waves (1-3) drive strong outflow at levels above about 23 km while smaller-scale waves (4-180) drive strongest outflow at levels below (Fig. 3c, d). The individual outflow induced by a single wave up to wave 59 can be seen in Fig. A1, which shows that, resolved waves with scale smaller than wave 6 are almost exclusively driving the shallow branch of the stratospheric circulation.

https://doi.org/10.5194/egusphere-2024-4088
Preprint. Discussion started: 21 January 2025

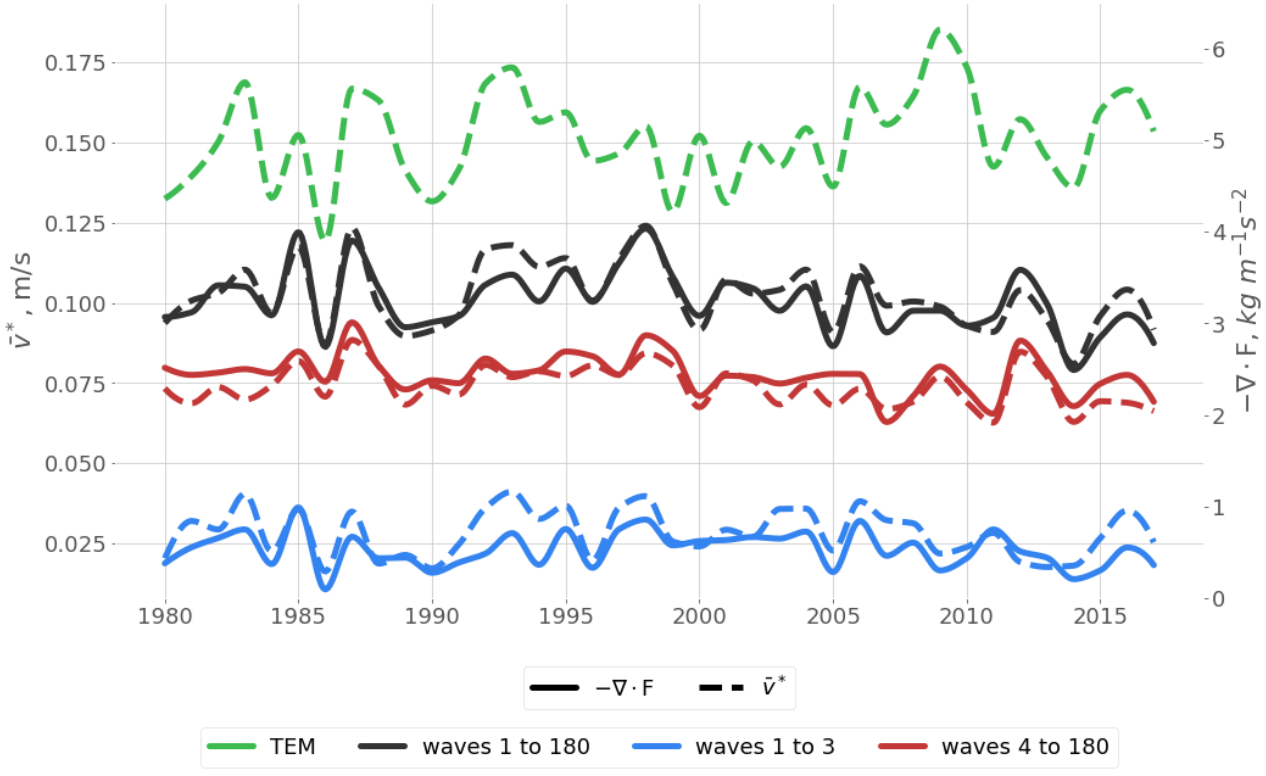

Figure 2. Annual mean time series at 70 hPa (mean 20N-40N) of horizontal component of the residual circulation (dashed lines), and divergence of Eliassen-Palm flux (solid lines). Residual velocity from Transformed Eulerian Mean (green), EPF divergence and residual velocities from downward control for total (black), large-scale (blue) and smaller-scale (red) waves. The figure is based on 1980-2017 ERA5 data

The role of waves with wavenumber 3 and 4 appears to be somewhat intermediate, with these waves driving a significant portion of the circulation at all levels. Yet, including wave 4 in the large-scale waves makes their drag to correlate better with outflow velocity in the shallow branch region in the southern hemisphere than the drag of the smaller-scale waves (blue line in Fig. 3b). Furthermore, adding wave 3 to the smaller-scale waves, makes their drag to correlate better with the outflow velocity at certain levels in the middle stratosphere compared to the large-scale waves (red lines in Fig. 3a, b). Regarding the relative outflow in Fig. 3d, waves with wavenumbers larger than 3 produce outflow maxima which are well-confined below about 25km, while the outflow due to larger-scale waves maximizes over broad regions above. Taking all these aspects into account, we define those large-scale planetary waves with wavenumber 1-3 as drivers of the deep branch and the smaller-scale waves (wavenumbers larger than 3) as drivers of the shallow branch. The following analyses of BDC structure, variability and trends, support our choice in separating the wave driving into 1-3 for the deep branch and larger than 3 for the shallow branch.

https://doi.org/10.5194/egusphere-2024-4088
Preprint. Discussion started: 21 January 2025

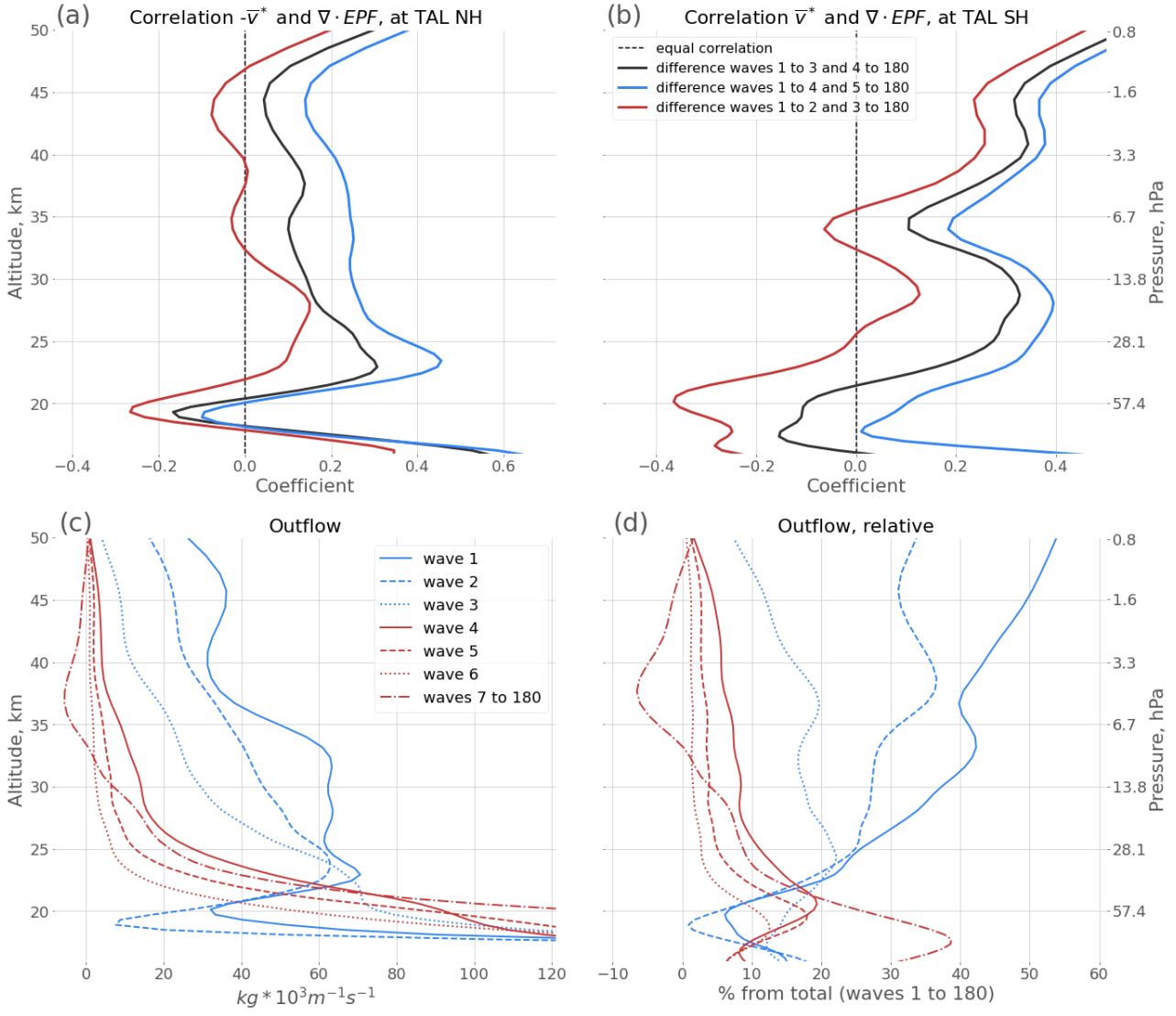

Figure 3. (a) Correlation between outflow velocity from TEM approach and wave drag generated by different wave bands (colors) at turn-around latitudes in the northern hemisphere. (b) Same as (a) but for the southern hemisphere. (c) Outflow from the area between TAL calculated from Downward Control principle for different waves (colors and line styles). (d) Equivalent to (c) but in relative units as percentage of the total outflow of all resolved waves. The lines presented in this figure were smoothed with a Gaussian filter for better readability. The figure is constructed from monthly mean ERA5 data for 1980-2017.

Vertical profiles of upwelling and outflow generated by waves with wavenumbers 1-3 and 4-180 were constructed for different reanalyses (Fig. 4). Regardless of the reanalysis, waves 1 to 3 generate the majority of the outflow in the middle stratosphere and nearly all of it in the upper stratosphere. Waves 4 to 180, on the other hand, are responsible for most of the

https://doi.org/10.5194/egusphere-2024-4088
Preprint. Discussion started: 21 January 2025

outflow in the lower stratosphere. Compared to the other three reanalyses, ERA5 data indicates a notably higher total outflow in the lower stratosphere between about 20-25km. This difference appears related to the effects of small-scale waves and the outflow they generate. Specifically, gravity waves (here defined as waves with wavenumbers 21-180) generate considerably greater drag in ERA5 than in the other reanalyses. The drag caused by waves 1 to 3 is very similar between all four reanalyses. Having higher resolution, ERA5 is able to resolve gravity waves better than other reanalyses. Consequently, in ERA5 these waves contribute significantly more to the shallow branch. Figure 4 further shows that the level which separates the two dynamical regimes with outflow mainly generated by large-scale waves above and mainly by small-scale waves below emerges similarly for the different reanalyses. Therefore, this level represents a natural separation in terms of dynamical characteristics, i.e. wave driving, between the shallow and deep branches of the stratospheric circulation and is largely consistent across the different datasets considered.

Consequently, we define the separation level between the deep and shallow branches as the lowest altitude at which the contribution to outflow from waves 1-3 is equal to the contribution from waves 4-180. To eliminate sharp spikes of outflow in monthly man data, which can cause unexpected variations in the separation level height, a rolling mean over five vertical levels is applied to the outflow profiles before determining the separation level. In cases where the monthly mean data shows equal contributions to the outflow from waves 1–3 and 4–180 at multiple altitudes, we consider the separation level too vague for accurate estimation and exclude these months.

Table 1. Mean seasonal cycle of the separation level height (hPa) calculated for different reanalyses over the period 1980-2017.

	Jan	Feb	Mar	Apr	May	Jun	Jul	Aug	Sep	Oct	Nov	Dec	mean
ERA5	41.03	41.49	43.35	40.02	42.68	49.98	45.23	45.59	42.00	39.95	40.88	42.20	42.78
ERA-Interim	41.87	42.34	43.87	49.38	45.21	52.44	50.66	50.95	50.00	41.58	40.07	41.39	45.61
JRA55	44.13	44.70	45.33	43.41	42.57	54.20	51.39	49.00	51.05	42.51	41.43	42.05	45.80
MERRA2	43.79	41.78	43.13	48.46	43.94	51.63	51.14	49.88	51.68	45.63	45.27	45.25	46.67

The seasonal variation of the separation level is shown in Fig. 5. The separation level shows a similar seasonal cycle in all four reanalyses considered, with a somewhat lower separation level height in boreal summer months. The separation level height depends on the relative contributions of large-scale waves 1-3 and small-scale waves 4-180 to tropical outflow. A stronger contribution from large-scale planetary waves raises the separation level, whereas a stronger contribution from smaller-scale waves lowers the separation level (Fig. 4d). Therefore, the seasonal cycle of the separation level is likely linked to the annual cycle of wave drag. In particular the weaker planetary wave activity during boreal summer appears important for pushing the separation level downward.

The large variability of the separation level (standard deviation, shown by the whiskers in Fig. 5) indicates a large inter-annual variation of the separation level height, which is of similar magnitude as the seasonal variation.

Furthermore, during most months the separation level is located at higher altitudes for ERA5 compared to other reanalyses (Fig. 5). It is likely the ability of ERA5 to better resolve small-scale waves which shifts the separation level to higher altitude

https://doi.org/10.5194/egusphere-2024-4088
Preprint. Discussion started: 21 January 2025

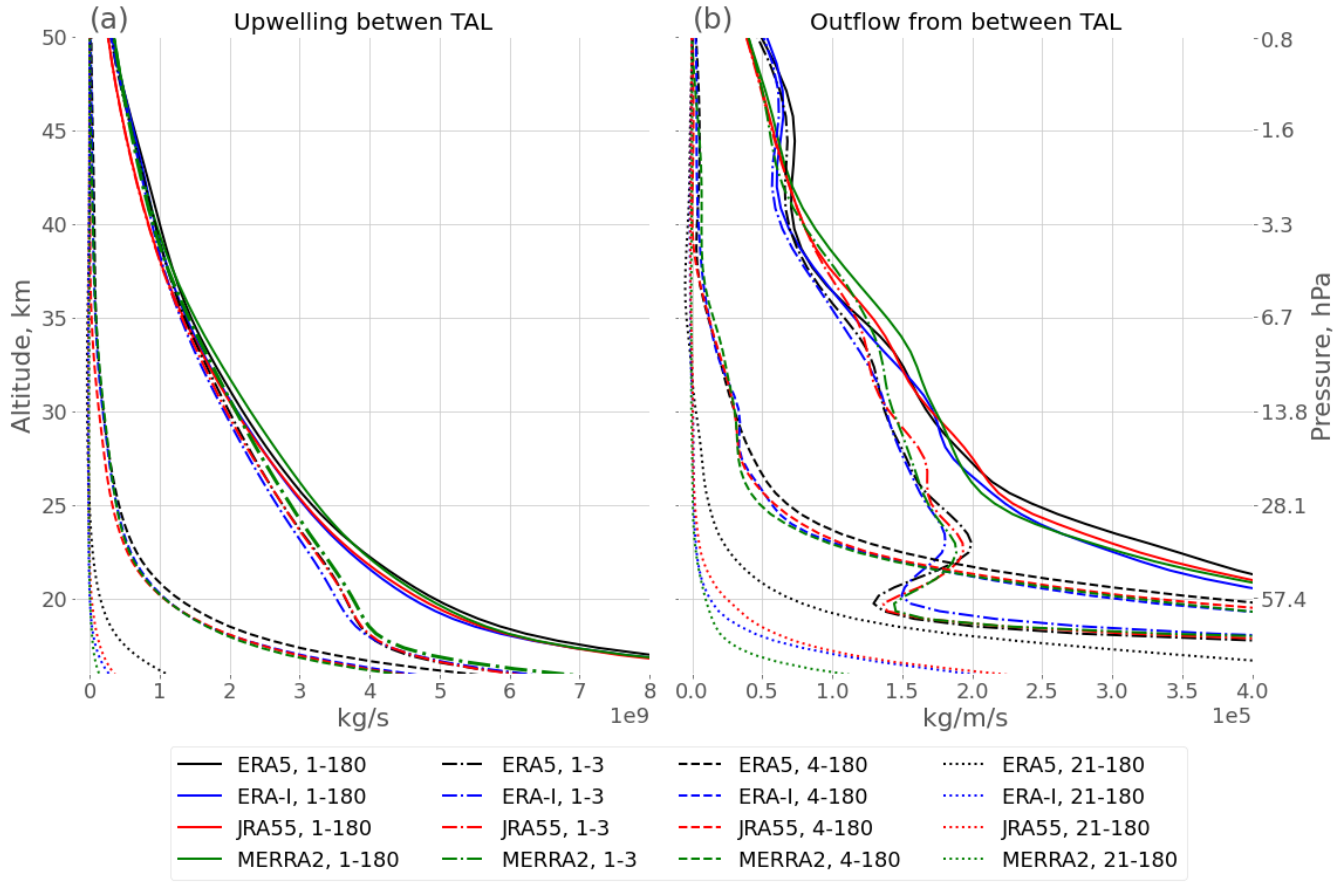

Figure 4. (a) Mean profiles of upwelling calculated from DWCP, induced by all waves (solid lines), waves 1-3 (dash-dotted lines), waves 4-180 (dashed lines), and waves 21-180 (dotted lines) from ERA5 (black), ERA-Interim (blue), JRA55 (red), and MERRA2 (green) reanalyses for 1980-2017. (b) Corresponding profiles of outflow (a). The lines presented in this figure were smoothed with a Gaussian filter for better readability.

compared to the other reanalyses. Given its higher resolution and ability to resolve larger parts of the gravity wave spectrum, the estimate of the separation level height from ERA5 is likely more accurate compared to the other reanalyses.

The focus of this study is on the effects of resolved waves, but we notice that contributions from small-scale, unresolved waves could modify our results. We expect a higher separation level if higher-resolution reanalyses were able to resolve more smaller-scale waves or if parameterized wave drag was added to the resolved wave drag.

https://doi.org/10.5194/egusphere-2024-4088
Preprint. Discussion started: 21 January 2025

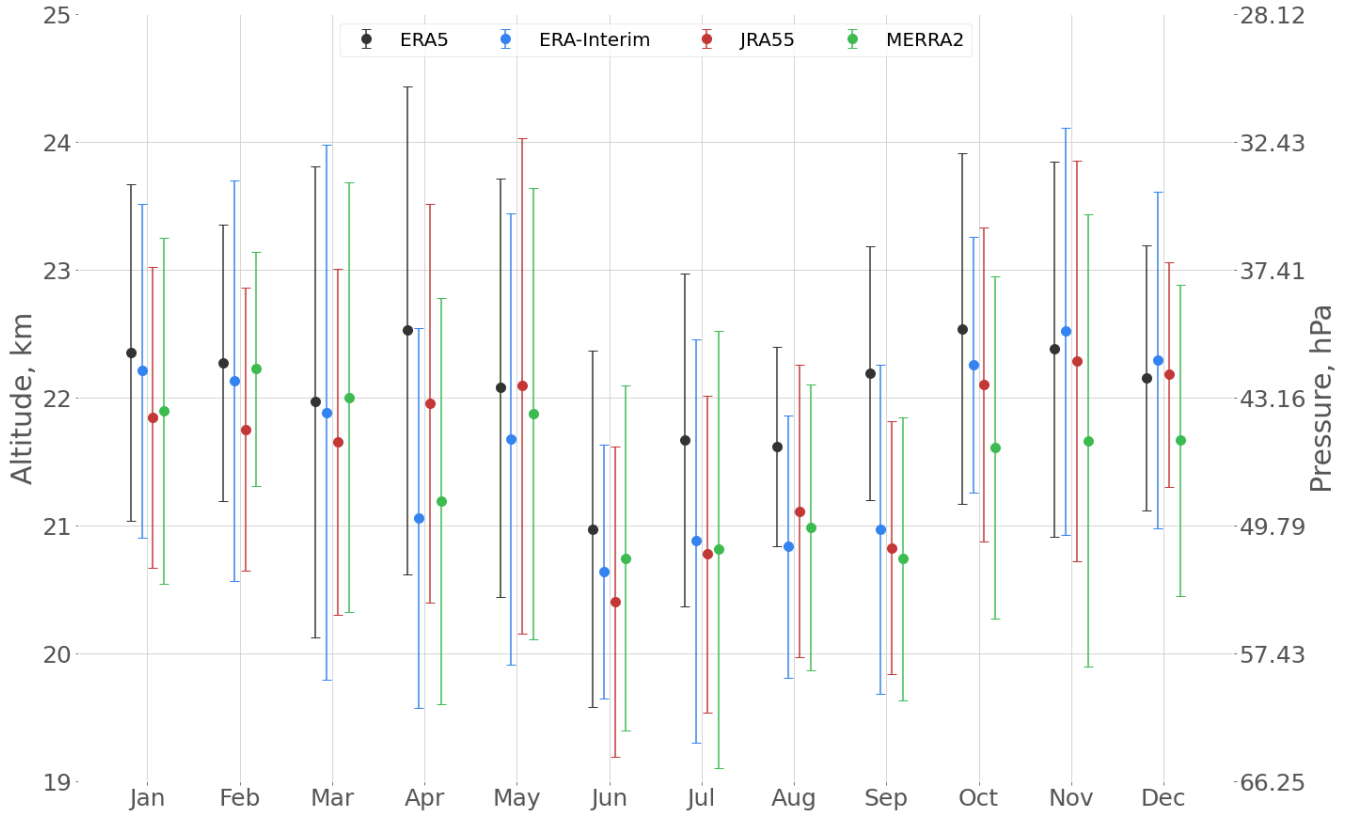

Figure 5. Seasonal cycle of the level separating the deep and shallow branches of the stratospheric circulation. Dots show the mean altitude of the level for each month, with the corresponding standard deviation as error bar. The colours represent different reanalyses: Era-Interim (blue), JRA55 (red) and MERRA2 (green). The level is estimated from 1980-2017 monthly mean data.

4 Variability and trends in circulation structure

Figure 6 shows the upwelling at 100 hPa which is close to the tropopause, at 43 hPa which is approximately the separation level between shallow and deep branch, and the difference between upwelling at 100 hPa and 43 hPa. The upwelling at the tropopause is related to the outflow at all levels above in the stratosphere (with a small portion of it even related to outflow at levels above the stratopause). Therefore, changes in upwelling at this level reflect changes in the overall overturning circulation. The ERA5 annual mean total upwelling generated by all resolved waves and estimated using the DWCP at 100 hPa is close to $1 * 10^{10}$ kg/s. The variability in the monthly mean upwelling is significant and has a standard deviation of $2.2 * 10^{9}$ kg/s (Table 2). At 100 hPa, the large-scale planetary waves (wavenumbers 1-3) and resolved smaller-scale waves contribute similarly to annual mean upwelling. Monthly mean upwelling caused by large-scale planetary wave drag has a standard deviation close

https://doi.org/10.5194/egusphere-2024-4088
Preprint. Discussion started: 21 January 2025

to the standard deviation of the upwelling caused by smaller-scale waves (Table 2). Therefore, both large-scale planetary and small-scale waves appear to contribute almost equally to the forcing and variability of the whole overturning circulation.

Lin et al. (2013) divided the stratospheric circulation into a deep branch (above 30 hPa), a shallow branch (between 70 hPa and 30 hPa) and a transitional branch (between 100 hPa and 70 hPa). Although the lowest layer (100-70 hPa) is still influenced by tropospheric processes, our results show no clear indication of wave driving differences for this layer compared to the layers above. Therefore, in the present study we aim at a dynamical separation of only the shallow and deep banches based on the circulation's wave driving.

Table 2. Mean upwelling and standard deviation of monthly mean upwelling in 10^9 kg/s. All values are based on ERA5 1980-2017 data.

	waves 1 to 180		waves 1 to 3		waves 4 to 180	
level	upwelling	σ	upwelling	σ	upwelling	σ
43 hPa	4.09	1.37	3.35	1.21	0.73	0.38
100 hPa - 43 hPa	5.79	1.80	1.91	1.08	3.88	1.32
100 hPa	9.88	2.24	5.27	1.61	4.61	1.36

The total outflow of the shallow branch can be estimated by subtracting the upwelling at the separation level (43 hPa) from the upwelling at the bottom of the stratosphere (100 hPa). In the layer between 100 and 43 hPa, the dissipation of the resolved waves generates an annual mean upwelling close to $5.8*10^9$ kg/s, about 2/3 of this upwelling being forced by the smaller-scale waves and only about 1/3 by large-scale planetary waves. Yet, with a monthly mean standard deviation of $1.1*10^9$ kg/s for large-scale planetary waves and $1.3*10^9$ kg/s for smaller-scale waves, both types of waves contribute similarly to the variability of the upwelling in that layer.

The upwelling across the mean separation level is generally a result of the wave drag in the deep branch region above that level. The annual mean of this upwelling across the separation level is about $4.1*10^9$ kg/s, the majority of which is caused by large-scale planetary waves and less than 20% by smaller-scale waves. The variability of the monthly mean upwelling across the separation level (43 hPa) is mostly controlled by large-scale planetary waves. This is indicated by the fact that variability (here standard deviation) of upwelling induced by large-scale planetary waves is about three times larger compared to the standard deviation of upwelling induced by smaller-scale waves (Table 2). Therefore, despite the clear separation in wave driving concerning the climatological mean circulation, both wave types contribute significantly to the circulation variability of the shallow branch, while the variability of the deep branch is mostly controlled by the large-scale planetary waves.

To further investigate the wave driving of the circulation variability, a vertical profile of the correlation coefficient between the outflow generated by all waves and the outflow only due to large-scale (1-3) and smaller-scale waves was constructed (Fig. 7). Across all four reanalyses, the correlation of total outflow with the contribution from only small-scale waves is largest at lower levels below about 25km. Hence, smaller-scale waves influence the variability mostly in the lower stratosphere. Large-scale planetary waves are relevant to the variability of the circulation throughout the stratosphere. Although, these large-

https://doi.org/10.5194/egusphere-2024-4088
Preprint. Discussion started: 21 January 2025

scale waves clearly dominate the variability in the middle and upper stratosphere (consistent with the standard deviation of upwelling shown in table 2), and their contribution to the variability weakens at levels below about 25km (Fig. 7). Overall, despite similar contributions to the mass flux across the tropical tropopause level (at about 100 hPa) from both types of waves, large-scale planetary waves in general contribute more to the overall variability of the circulation. The higher impact of large-scale planetary waves on the variability of the circulation is possibly related to the fact that, the standard deviation of the upwelling at 100 hPa takes into account changes in the wave drag from that level and all levels above (see Sect. 2). Filtering by the background wind according to the Charney-Drazin criterion (Eq. 9) more strongly affects the smaller-scale waves, hinders their upward propagation and therefore dampens their contribution to circulation forcing at upper levels. Hence, wave drag of the large-scale planetary waves is distributed over a larger altitude range in the stratosphere than the wave drag of the smaller-scale waves. Consequently, large-scale planetary waves significantly contribute to the variability of the circulation at all levels and smaller-scale waves only affect the circulation variability in the shallow branch region.

Multi-decadal trends in the upwelling over the period 1980–2017 are presented in Fig. 8. Given the relatively short time period for trend calculation, upwelling trends are mostly not statistically significant at 95% confidence level. The trends of upwelling estimated from the TEM residual circulation velocity (black dotted lines in Fig. 8) and from the DWCP (black solid lines in Fig. 8) may be significantly different. While here, we mostly focus on the resolved wave drag, the majority of past studies are focussing on the total upwelling from the TEM velocities (e.g. Fujiwara et al., 2021). Hence, most published results need to be compareed to the TEM-based estimate (black dotted lines in Fig. 8). However, consistent patterns in the trend profiles emerge for the different reanalyses. Above 25 km, the upwelling trend estimated from the total wave drag is positive and S-shaped for all four reanalyses with a local trend maximum around 35km. Strongest differences to the other reanalyses are found for MERRA2. In particular, at lower levels the shallow branch trend is mostly weakly positive for MERRA2, but negative for the other three reanalyses. For ERA5, ERA-Interim and JRA55 the deep branch trend is largely driven by large-scale planetary waves while for MERRA2 smaller-scale waves also contribute significantly to the trend. Furthermore, MERRA2 has a generally more positive trend of upwelling driven by smaller-scale waves than that driven by large-scale planetary waves below about 30km, which is opposite to the other three reanalyses. For most reanalyses and levels the agreement between trends of upwelling estimated from the total resolved wave drag and from the TEM approach is poor. Only for ERA5 the trend from resolved wave drag matches the total TEM velocity-based trend well between about 23-35km. Also, ERA5 is the only reanalysis where the trend in the shallow branch is almost exclusively controlled by the smaller-scale waves, and which shows a significant contribution of resolved gravity waves (wavenumber larger 20) to the overall shallow branch trend.

The robust difference in the dominant contribution of large-scale and small-scale waves to the upwelling trends above and below about 23km (Fig. 8) corroborates our wave drag-based estimate of the separation level between the shallow and deep branch layers. In particular, different trends in dynamics are apparent in different altitude regions, indicating a decoupling of the two circulation branches regarding their long-term evolution. These differences in trends between the shallow and deep branch are consistent, at least qualitatively, for the different reanalyses.

As noted before, the upwelling at a given level is driven by the wave drag at the level and all levels above it and hence the upwelling trend at a given level is not related unambiguously to wave drag changes only at that level. A clearer relation to wave

https://doi.org/10.5194/egusphere-2024-4088
Preprint. Discussion started: 21 January 2025

drag changes at a given level holds for changes in meridional outflow at that level. Trend profiles for outflow are presented in Fig. 9 for the four different reanalyses and separated into contributions from small-scale and large-scale planetary waves. Given the relation to upwelling in Eq. 8, trends in outflow are directly related to the vertical derivative of the trends in upwelling. Therefore, the outflow trends are positive in a shallow layer above the tropical tropopause. Above, outflow shows generally negative trends throughout a broad layer between about 18-35km (somewhat depending on the reanalysis considered), and indicating weakening of transport out of the tropics in that altitude region. Above about 35km, outflow increases throughout an about 5km thick layer, consistent with the negative vertical gradient in upwelling trends in Fig. 8. Whereas most of the reanalysis-based trends are statistically insignificant, we hypothesize that the robust vertical pattern, with outflow weakening below and strengthening above about 35km, could be indicative for an upward shift of the deep branch of the stratospheric circulation. Another robust vertical pattern is the strengthening of outflow in the lower part of the shallow branch and weakening above, which could be indicative for a downward shift of the shallow branch of the stratospheric circulation. Overall, longer timeseries are needed to deduce robust long-term trends of the stratospheric circulation from reanalysis data.

Given the limited period of the analyzed data and large inter-annual variability of the separation level height, the trend of the separation level for any of the reanalyses is smaller than two standard errors and therefore is not significantly different from zero. However, three out of four reanalyses have negative trends of the separation level height, while only JRA55 has a slightly positive trend (Fig. 10). The negative trend of the separation level can also be estimated from Fig. 9, which shows that the trend of large scale waves is generally more positive than the trend of small scale waves around the separation level. Hence the contribution of large-scale planetary waves around the separation level increases over time compared to the contribution of smaller-scale waves, and consequently pushes the separation level slightly downwards.

5 Discussion

The stratospheric circulation is usually separated into a deep and a shallow branch. However, different metrics have been used in past studies to separate these circulation branches. Some studies applied a separation by a selection of a boundary pressure level which splits the upwelling mass flux approximately into a specific ratio between the deep and shallow branch, e.g. ∼50 hPa proposed by Ball et al. (2016) or 30 hPa proposed by Lin et al. (2013); Diallo et al. (2019). Since vertical velocities in the stratosphere are much weaker than horizontal ones, transit times from the stratospheric entry point at the tropical tropopause to the downwelling region in the extratropical lowermost stratosphere along the shallow branch are significantly lower than along the deep branch. Based on this difference in transit time, a separation between deep and shallow circulation branches has also been proposed based on transit times along residual circulation trajectories (Birner and Bönisch, 2011). Furthermore, the transport of air masses from the so-called “tropically controlled transition region” with an upper boundary at about 450K (approximately 70 hPa) into the extratropics appears to be related to the shallow branch (Rosenlof et al., 1997; Bönisch et al., 2009; Bönisch et al., 2011). In view of such diversity in the published approaches to define a separation between the shallow and the deep stratospheric circulation branch, here we aim for a dynamical separation based on differences in the circulation’s wave driving inferred from reanalysis data. The robustness of our results is estimated from comparison of four different reanalyses.

https://doi.org/10.5194/egusphere-2024-4088
Preprint. Discussion started: 21 January 2025

It is established that the deep branch is associated with large-scale planetary waves breaking in the subtropical middle and upper stratosphere and the shallow branch is associated with synoptic and planetary waves breaking in the subtropical lower stratosphere (e.g. Plumb, 2002). Deploying a statistical and a mechanistic method, we find that in current global reanalyses the outflow in the deep branch is indeed largely driven by large-scale planetary waves with wavenumbers 1-3. Waves with wavenumbers 4-6 have a somewhat noticeable contribution to the lower part of the deep branch. The shallow branch however, is mainly driven by smaller-scale Rossby waves (wavenumbers 4 to 20) and to a lesser extent by small-scale gravity waves (wavenumber larger than 20). It should be noted, that due to coarse resolution in the current generation reanalyses the contribution of gravity waves in our study is likely underestimated, as also suggested by a significant DWCP upwelling deficit in our study (see Fig. A2, and also (Butchart et al., 2011)). For the resolved waves considered here, however, the wave drag-based separation of the deep and the shallow branch is robust across all four reanalyses used.

The mean level separating the deep and the shallow branch of the residual circulation is located between 43 and 47 hPa depending on the reanalysis. Hence, despite using different arguments the separation level found in this work is close to the levels estimated in past studies. Moreover, this separation level between the two circulation branches was found to have an annual cycle, with lowest separation level during boreal summer, which is similar in all reanalyses used in this work. Both the inter-annual and seasonal variability of the separation level have an amplitude which is larger than the differences between the reanalyses.

Most of the residual circulation trends estimated in this work are within two standard errors around zero and therefore are not statistically significant. Yet there are patterns which robustly emerge in all reanalyses used, as an acceleration of upwelling above 28 hPa, and mostly negative trends of outflow between 60 and 15 hPa. Remarkably, also the planetary wave contribution to the trends varies considerably between reanalyses, and thus also large-scale waves appear not well enough constrained in reanalyses when it comes to trends. It should be noted that this study focused only on the resolved wave drag. Depending on the reanalysis, inclusion of the parameterized wave drag could noticeably alter the results by increasing the contribution to the circulation from smaller-scale waves, which likely pushes the separation level upward.

The reanalyses data used here were down-sampled to 1x1 degree horizontal resolution and 6-hour temporal resolution. This down-sampling to lower spatial resolution did not significantly affect the large-scale features of the residual circulation considered here (see Fig. A4 and Fig. A5). As also shown by Seviour et al. (2011), from a climatological monthly-mean perspective the 6-hourly data is sufficient to take tidal effects into account. However, if 6 hours resolution is used, some distortions remain in monthly mean data when $\bar{w}^*$ is considered, and there is little to no distortion remain when $\nabla \cdot EPF$ is considered. Regarding daily mean data for specific dates, reducing the temporal resolution from 1 to 6 hours had significant impact on the representation of the residual circulation. Therefore, in order to investigate short-term and smaller-scale features of the circulation it could be crucial to have higher temporal resolution. Yet, overall features of the circulation on a monthly mean time scale were not affected much by the down-sampling.

Vertical profiles of upwelling estimated using the TEM approach for all four reanalyses are shown in Fig. A2 together with the difference to the DWCP upwelling estimate ($(W - W_D)/W * 100\%$ denoted relative "upwelling deficit" in the following), which quantifies the contribution of parameterized wave drag to the upwelling. For all four reanalyses, the vertical profile of

https://doi.org/10.5194/egusphere-2024-4088
Preprint. Discussion started: 21 January 2025

the upwelling deficit shows a C-like shape with higher deficit in the lowest and highest parts of the stratosphere. The C-like shape of the deficit indicates that, the parameterized wave drag in the reanalyses mostly affects lowest and highest parts of the stratosphere, which is expected due to gravity wave drag being significantly stronger in the lower and upper stratosphere than in the middle stratosphere. Due to its higher resolution and greater ability to resolve gravity waves, ERA5 has significantly stronger resolved gravity wave drag as shown in Fig. 4 in Sect. 3. Thus, ERA5 has the smallest upwelling deficit at the bottom of the stratosphere. Also in the upper stratosphere, a significant part of upwelling appears to be related to unresolved gravity waves (Plumb, 2002). Also at these upper levels at the top of the stratosphere, the upwelling deficit in ERA5 is significantly smaller than in the other reanalyses. In the middle stratosphere the difference between ERA5, MERRA2 and ERA-Interim is small. Throughout the stratosphere, JRA55 shows the largest deficit among all four reanalyses considered.

Furthermore, ERA5 shows the strongest total resolved upwelling and outflow (from DWCP) at the bottom of the stratosphere (see Fig. A3b). This indicates that the total resolved wave drag is about 5 to 10% greater in ERA5 than in the other reanalyses. The total TEM-based upwelling at the same altitude, including effects from parameterized waves, is significantly weaker in ERA5 than in ERA-Interim or JRA55, therefore results are consistent with Ploeger et al. (2021). At the top of the stratosphere, the TEM upwelling in ERA5 is 20 to 30% weaker than in the other reanalyses (see Fig. A3a).

In general, the upwelling based on the different reanalysis is more similar when estimated from resolved waves only (Fig. A3a, b). Therefore, in this paper we mainly focus on the circulation driven by the resolved wave drag. Furthermore, differences between the reanalyses may indicate significant differences in the gravity wave parameterization. In particular, ERA5 has generally stronger upwelling estimated from the resolved wave drag and weaker TEM upwelling in the regions where the effect of small-scale gravity wave drag on the circulation is expected to be strongest. Therefore, the smaller DWCP upwelling deficit in ERA5 is likely due to a better ability to resolve the waves and from weaker parameterized wave drag.

6 Conclusions

Based on both a statistical and a mechanistic approach we here propose a dynamical separation of the deep and shallow branches in the stratospheric circulation. We find that the deep branch is mainly driven by large-scale planetary waves with wavenumbers 1 to 3 and shallow branch by smaller-scale waves with wavenumber larger than 3. The mean altitude of the level separating the deep and shallow branch is at about 43 hPa with significant inter-annual and seasonal variations. In particular, the separation level height shows a clear semi-annual cycle in all four reanalyses. The dynamical separation criterion found in this work appears robust across all four reanalyses used in this work.

At the tropical tropopause, both wave types (wavenumbers 1-3 and 4-180) generate roughly half of the upwelling (blue and red line in Fig. 6a), and both branches of the overturning circulation move a similar amount of mass (black lines in Fig. 6 b and c). While the variability of the deep branch is mostly controlled by large-scale planetary waves, both large-scale planetary and smaller-scale waves affect the variability of the shallow branch to a similar extent.

https://doi.org/10.5194/egusphere-2024-4088
Preprint. Discussion started: 21 January 2025

The circulation trends over the period 1980-2017 estimated here for the different reanalyses were found not to be statistically significant. However some of the trend features, like an acceleration of the circulation at altitudes of about 35-40 km emerged robustly from all four reanalyses.

Given the differences between reanalyses regarding the climatological height, variability and trends in the separation level, for detailed investigations of the structure of the stratospheric circulation a precise identification of the separation level is needed. In particular, calculating the specific separation level for the given dataset, e.g. as proposed here from wave drag, appears advantageous. Otherwise, we recommend using the separation level calculated here from ERA5 (Table 1), due to the better ability of that reanalysis to represent effects of small-scale waves.

It should further be noted that the 70 hPa level, which is often used as a reference level for model inter-comparisons of stratospheric tropical upwelling, is not unambigously related to a distinct circulation branch but is indeed affected by both the deep and the shallow branch. As shown here, the separation level between these circulation branches may significantly differ between different models, and so may the effects of the deep and shallow branch on upwelling across 70 hPa. Using the appropriate separation levels for distinguishing the deep and shallow branch in model and reanalysis inter-comparisons could reduce the spread between models regarding climatology and trends in the stratospheric circulation.

. *Data availability.* The ERA5, reanalysis data are processed by the European Centre for Medium-Range Weather Forecasts and available from the Climate Data Store (https://cds.climate.copernicus.eu/). The JRA55 reanalysis data are processed by the Japan Meteorological Agency and available from the Data Integration and Analysis System Program (https://diasjp.net/en/). The MERRA2 data are processed by the NASA Goddard Global Modeling and Assimilation Office and available from the Data and Information Services Center (https://disc.gsfc.nasa.gov/).

. *Author contributions.* RB carried data processing and analysis. FP contributed code for the analysis. FP, PP, ME, and TB provided helpful discussions and contributed to the design of the analysis.

. *Competing interests.* The authors declare that they have no conflict of interest.

. *Financial support.* The article processing charges for this open-access publication were covered by the Forschungszentrum Jülich.

. *Acknowledgements.* FP acknowledges support by the Deutsche Forschungsgemeinschaft (DFG, German Research Foundation) – TRR 301 – project ID 428312742. Finally, we gratefully acknowledge the computing time for the CLaMS simulations which was granted on the supercomputer JUWELS at the Jülich Supercomputing Centre (JSC) under the VSR project ID CLAMS-ESM.

https://doi.org/10.5194/egusphere-2024-4088
Preprint. Discussion started: 21 January 2025

Appendix A

https://doi.org/10.5194/egusphere-2024-4088
Preprint. Discussion started: 21 January 2025

References

Abalos, M., Legras, B., Ploeger, F., and Randel, W. J.: Evaluating the advective Brewer-Dobson circulation in three reanalyses for the period 1979-2012, J. Geophys. Res., 120, doi:10.1002/2015JD023 182, 2015.

Abalos, M., Calvo, N., Benito-Barca, S., Garny, H., Hardiman, S. C., Lin, P., Andrews, M. B., Butchart, N., Garcia, R., Orbe, C., Saint-Martin, D., Watanabe, S., and Yoshida, K.: The Brewer–Dobson circulation in CMIP6, Atmos. Chem. Phys., 21, 13 571–13 591, https://doi.org/10.5194/acp-21-13571-2021, https://acp.copernicus.org/articles/21/13571/2021/, 2021.

Andrews, D. G., Holton, J. R., and Leovy, C. B.: Middle Atmosphere Dynamics, Academic Press, San Diego, USA, 1987.

Ball, W. T., Kuchař, A., Rozanov, E. V., Staehelin, J., Tummon, F., Smith, A. K., Sukhodolov, T., Stenke, A., Revell, L., Coulon, A., Schmutz, W., and Peter, T.: An upper-branch Brewer–Dobson circulation index for attribution of stratospheric variability and improved ozone and temperature trend analysis, Atmos. Chem. Phys., 16, 15 485–15 500, https://doi.org/10.5194/acp-16-15485-2016, 2016.

Birner, T. and Bönisch, H.: Residual circulation trajectories and transit times into the extratropical lowermost stratosphere, Atmos. Chem. Phys., 11, 817–827, https://doi.org/10.5194/acp-11-817-2011, 2011.

Bönisch, H., Engel, A., Curtius, J., Birner, T., and Hoor, P.: Quantifying transport into the lowermost stratosphere using simultaneous in-situ measurements of SF_6 and CO_2, Atmos. Chem. Phys., 9, 5905–5919, 2009.

Bönisch, H., Engel, A., Birner, T., Hoor, P., Tarasick, D. W., and Ray, E. A.: On the structural changes in the Brewer-Dobson circulation after 2000, Atmos. Chem. Phys., 11, 3937–3948, https://doi.org/10.5194/acp-11-3937-2011, 2011.

Butchart, N.: The Brewer-Dobson circulation, Rev. Geophys., 52, 157–184, https://doi.org/10.1002/2013RG000448, 2014.

Butchart, N., Charlton-Perez, A. J., Cionni, I., Hardiman, S. C., Haynes, P. H., Krueger, K., Kushner, P. J., Newman, P. A., Osprey, S. M., Perlwitz, J., Sigmond, M., Wang, L., Akiyoshi, H., Austin, J., Bekki, S., Baumgaertner, A., Braesicke, P., Bruehl, C., Chipperfield, M., Dameris, M., Dhomse, S., Eyring, V., Garcia, R., Garny, H., Joeckel, P., Lamarque, J.-F., Marchand, M., Michou, M., Morgenstern, O., Nakamura, T., Pawson, S., Plummer, D., Pyle, J., Rozanov, E., Scinocca, J., Shepherd, T. G., Shibata, K., Smale, D., Teyssedre, H., Tian, W., Waugh, D., and Yamashita, Y.: Multimodel climate and variability of the stratosphere, J. Geophys. Res. A, 116, https://doi.org/10.1029/2010JD014995, 2011.

Chabrillat, S., Vigouroux, C., Christophe, Y., Engel, A., Errera, Q., Minganti, D., Monge-Sanz, B. M., Segers, A., and Mahieu, E.: Comparison of mean age of air in five reanalyses using the BASCOE transport model, Atmospheric Chemistry and Physics, 18, 14 715–14 735, https://doi.org/10.5194/acp-18-14715-2018, https://www.atmos-chem-phys.net/18/14715/2018/, 2018.

Charlesworth, E., Plöger, F., Birner, T., Baikhadzhaev, R., Abalos, M., Abraham, N. L., Akiyoshi, H., Bekki, S., Dennison, F., Jöckel, P., Keeble, J., Kinnison, D., Morgenstern, O., Plummer, D., Rozanov, E., Strode, S., Zeng, G., Egorova, T., and Riese, M.: Stratospheric water vapor affecting atmospheric circulation, Nat. Commun., 14, 3925, https://doi.org/https://doi.org/10.1038/s41467-023-39559-2, 2023.

Charney, J. G. and Drazin, P. G.: Propagation of planetary-scale disturbances from the lower into the upper atmosphere, J. Geophys. Res., 66, 83–109, https://doi.org/10.1029/JZ066i001p00083, http://dx.doi.org/10.1029/JZ066i001p00083, 1961.

Dee, D. P., Uppala, S. M., Simmons, A. J., Berrisford, P., Poli, P., Kobayashi, S., Andrae, U., Balmaseda, M. A., Balsamo, G., Bauer, P., Bechtold, P., Beljaars, A. C. M., van de Berg, L., Bidlot, J., Bormann, N., Delsol, C., Dragani, R., Fuentes, M., Geer, A. J., Haimberger, L., Healy, S. B., Hersbach, H., Hólm, E. V., Isaksen, L., Kållberg, P., Köhler, M., Matricardi, M., McNally, A. P., Monge-Sanz, B. M., Morcrette, J.-J., Park, B.-K., Peubey, C., de Rosnay, P., Tavolato, C., Thépaut, J.-N., and Vitart, F.: The ERA-Interim reanalysis:

https://doi.org/10.5194/egusphere-2024-4088
Preprint. Discussion started: 21 January 2025

configuration and performance of the data assimilation system, Q. J. R. Meteorol. Soc., 137, 553–597, https://doi.org/10.1002/qj.828, 2011.

Diallo, M., Konopka, P., Santee, M. L., Müller, R., Tao, M., Walker, K. A., Legras, B., Riese, M., Ern, M., and Ploeger, F.: Structural changes in the shallow and transition branch of the Brewer–Dobson circulation induced by El Niño, Atmos. Chem. Phys., 19, 425–446, https://doi.org/10.5194/acp-19-425-2019, https://www.atmos-chem-phys.net/19/425/2019/, 2019.

Eluszkiewicz, J., Hemler, R., Mahlman, J., Bruhwiler, L., and Takacs, L.: Sensitivity of age-of-air calculations to the choice of advection scheme, J. Atmos. Sci., 57, 3185–3201, 2000.

Fujiwara, M., Manney, G. L., Gray, L. J., and Wright, J. S., eds.: SPARC Reanalysis Intercomparison Project (S-RIP) Final Report, SPARC Report No. 10, WCRP-6/2021, https://doi.org/10.17874/800dee57d13, 2021.

Garny, H., Ploeger, F., Abalos, M., Bönisch, H., Castillo, A. E., von Clarmann, T., Diallo, M., Engel, A., Laube, J. C., Linz, M., Neu, J. L., Podglajen, A., Ray, E., Rivoire, L., Saunders, L. N., Stiller, G., Voet, F., Wagenhäuser, T., and Walker, K. A.: Age of Stratospheric Air: Progress on Processes, Observations, and Long-Term Trends, Reviews of Geophysics, 62, e2023RG000 832, https://doi.org/https://doi.org/10.1029/2023RG000832, https://agupubs.onlinelibrary.wiley.com/doi/abs/10.1029/2023RG000832, e2023RG000832 2023RG000832, 2024.

Gelaro, R., McCarty, W., Suárez, M. J., Todling, R., Molod, A., Takacs, L., Randles, C. A., Darmenov, A., Bosilovich, M. G., Reichle, R., Wargan, K., Coy, L., Cullather, R., Draper, C., Akella, S., Buchard, V., Conaty, A., da Silva, A. M., Gu, W., Kim, G.-K., Koster, R., Lucchesi, R., Merkova, D., Nielsen, J. E., Partyka, G., Pawson, S., Putman, W., Rienecker, M., Schubert, S. D., Sienkiewicz, M., and Zhao, B.: The Modern-Era Retrospective Analysis for Research and Applications, Version 2 (MERRA-2), jci, 30, 5419–5454, 2017.

Gerber, E. P.: Stratospheric versus Tropospheric Control of the Strength and Structure of the Brewer-Dobson Circulation, J. Atmos. Sci., 69, 2857–2877, 2012.

Haynes, P. H., Marks, C. J., McIntyre, M. E., Shepherd, T. G., and Shine, K. P.: On the “downward control” of extratropical diabatic circulations by eddy-induced mean zonal forces., J. Atmos. Sci., 48, 651–678, 1991.

Hersbach, H., Bell, B., Berrisford, P., Hirahara, S., Horànyi, A., Muñoz Sabater, J., Nicolas, J., Peubey, C., Radu, R., Schepers, D., Simmons, A., Soci, C., Abdalla, S., Abellan, X., Balsamo, G., Bechtold, P., Biavati, G., Bidlot, J., Bonavita, M., De Chiara, G., Dahlgren, P., Dee, D., Diamantakis, M., Dragani, R., Flemming, J., Forbes, R., Fuentes, M., Geer, A., Haimberger, L., Healy, S., Hogan, R. J., Hólm, E., Janisková, M., Keeley, S., Laloyaux, P., Lopez, P., Lupu, C., Radnoti, G., de Rosnay, P., Rozum, I., Vamborg, F., Villaume, S., and Thépaut, J.-N.: The ERA5 global reanalysis, Q. J. R. Meteorol. Soc., 146, 1999–2049, https://doi.org/10.1002/qj.3803, 2020.

Holton, J. R., Haynes, P., McIntyre, M. E., Douglass, A. R., Rood, R. B., and Pfister, L.: Stratosphere-troposphere exchange, Rev. Geophys., 33, 403–439, 1995.

Kobayashi, S., Ota, Y., Harada, Y., Ebita, A., Moriya, M., Onoda, H., Onogi, K., Kamahori, H., Kobayashi, C., Endo, H., Miyaoka, K., and Takahashi, K.: The JRA–55 Reanalysis: General specifications and basic characteristics, J. Meteorol. Soc. Jpn., 93, 5–48, 2015.

Lin, J., Brunner, D., Gerbig, C., Stohl, A., Luhar, A., and Webley, P., eds.: Lagrangian Modeling of the Atmosphere, vol. 200, American Geophysical Union, Washington, DC, 2013.

Mahieu, E., Chipperfield, M. P., Notholt, J., Reddmann, T., Anderson, J., Bernath, P. F., Blumenstock, T., Coffey, M. T., Dhomse, S. S., Feng, W., Franco, B., Froidevaux, L., Griffith, D. W. T., Hannigan, J. W., Hase, F., Hossaini, R., Jones, N. B., Morino, I., Murata, I., Nakajima, H., Palm, M., Paton-Walsh, C., III, J. M. R., Schneider, M., Servais, C., Smale, D., and Walker, K. A.: Recent Northern Hemisphere stratospheric HCl increase due to atmospheric circulation changes, Nature, 515, 104–107, https://doi.org/10.1038/nature13857, 2014.

https://doi.org/10.5194/egusphere-2024-4088
Preprint. Discussion started: 21 January 2025

Ploeger, F., Legras, B., Charlesworth, E., Yan, X., Diallo, M., Konopka, P., Birner, T., Tao, M., Engel, A., and Riese, M.: How robust are stratospheric age of air trends from different reanalyses?, Atmos. Chem. Phys., 19, 6085–6105, https://doi.org/10.5194/gmd-12-2441-2019, 2019.

Ploeger, F., Diallo, M., Charlesworth, E., Konopka, P., Legras, B., Laube, J. C., Grooß, J.-U., Günther, G., Engel, A., and Riese, M.: The stratospheric Brewer–Dobson circulation inferred from age of air in the ERA5 reanalysis, Atmos. Chem. Phys. Discuss., pp. 1–27, https://doi.org/10.5194/acp-2020-1253, https://acp.copernicus.org/preprints/acp-2020-1253/, 2021.

Plumb, R. A.: Stratospheric transport, J. Meteorol. Soc. Jpn., 80, 793–809, 2002.

Ray, E. A., Moore, F. L., Rosenlof, K. H., Davis, S. M., Sweeney, C., Tans, P., Wang, T., Elkins, J. W., Boenisch, H., Engel, A., Sugawara, S., Nakazawa, T., and Aoki, S.: Improving stratospheric transport trend analysis based on SF_6 and CO_2 measurements, J. Geophys. Res., 119, 14 110–14 128, 2014.

Riese, M., Ploeger, F., Rap, A., Vogel, B., Konopka, P., Dameris, M., and Forster, P.: Impact of uncertainties in atmospheric mixing on simulated UTLS composition and related radiative effects, J. Geophys. Res., 117, D16305, https://doi.org/10.1029/2012JD017751, 2012.

Rosenlof, K. H., Tuck, A. F., Kelly, K. K., Russell III, J. M., and McCormick, M. P.: Hemispheric asymmetries in the water vapor and inferences about transport in the lower stratosphere, J. Geophys. Res., 102, 13 213–13 234, https://doi.org/10.1029/97JD00873, 1997.

Seviour, W. J. M., Butchart, N., and Hardiman, S. C.: The Brewer-Dobson circulation inferred form ERA-Interim, Q. J. R. Meteorol. Soc., 138, 878–888, 2011.

Solomon, S., Rosenlof, K., Portmann, R., Daniel, J., Davis, S., Sanford, T., and Plattner, G.-K.: Contributions of stratospheric water vapor to decadal changes in the rate of global warming, Science, 327, 1219–1223, https://doi.org/10.1126/science.1182488, 2010.

Stiller, G. P., Fierli, F., Ploeger, F., Cagnazzo, C., Funke, B., Haenel, F., Reddmann, T., Riese, M., and von Clarmann, T.: Shift of subtropical transport barriers explains observed hemispheric asymmetry of decadal trends of age of air, Atmos. Chem. Phys., 17, 11 177–11 192, 2017.

Vallis, G. K.: Atmospheric and oceanic fluid dynamics, Cambridge University Press, 2006.

Waugh, D. W.: The age of stratospheric air, Nature Geoscience, 2, 14–16, 2009.

Waugh, D. W. and Hall, T. M.: Age of stratospheric air: Theory, observations, and models, Rev. Geophys., 40, 1–27, 2002.

https://doi.org/10.5194/egusphere-2024-4088
Preprint. Discussion started: 21 January 2025

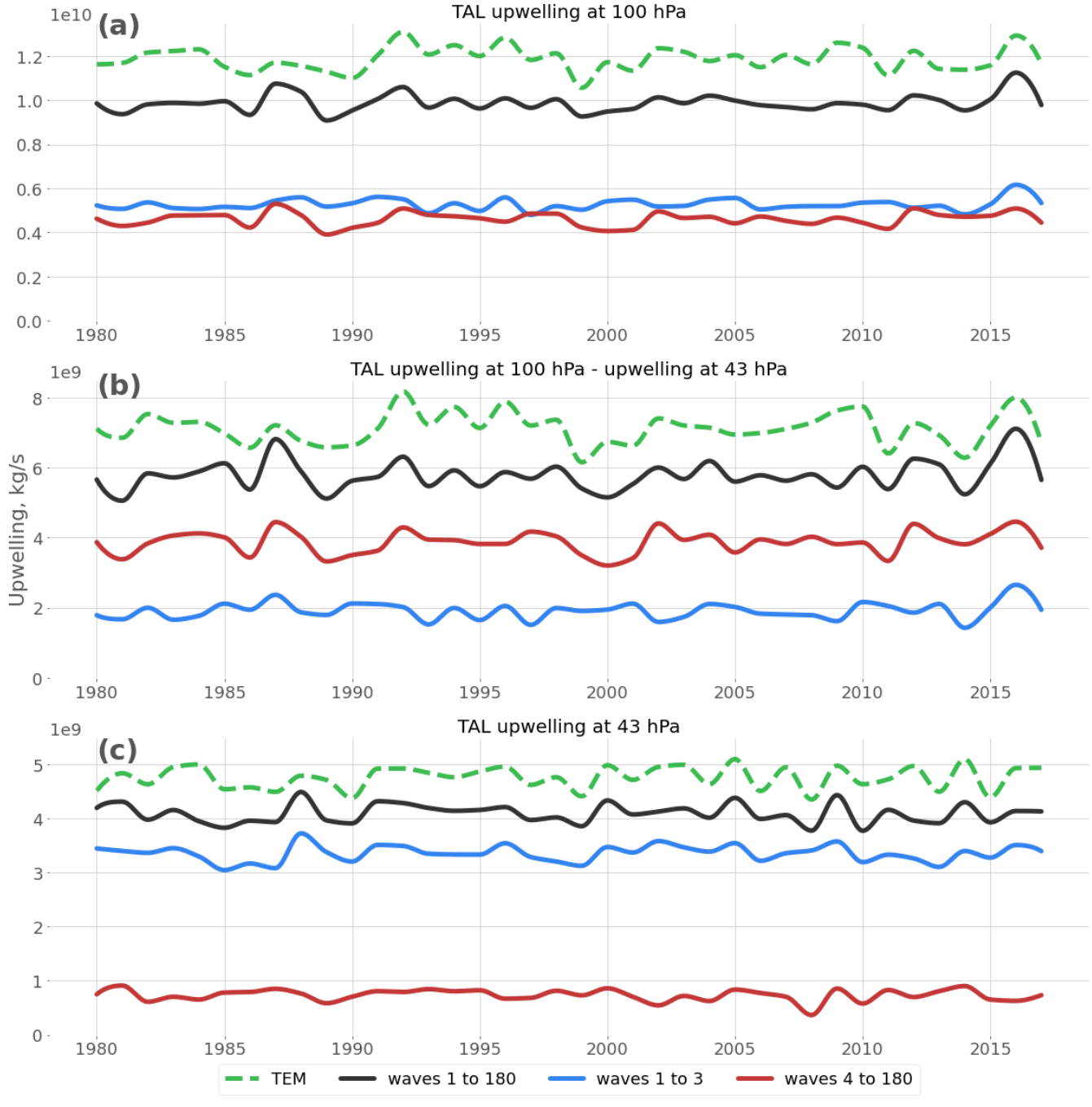

Figure 6. (a) Annual mean 1980-2017 time series of upwelling at 100 hPa from TEM approach (green), generated by total (black), large-scale planetary (blue), and smaller-scale (red) waves. (b) Difference between upwelling at 70 hPa and at 43 hPa, same legend as (a). (c) Upwelling at 43 hPa, same legend as (a). The figure is based on ERA5 data

https://doi.org/10.5194/egusphere-2024-4088
Preprint. Discussion started: 21 January 2025

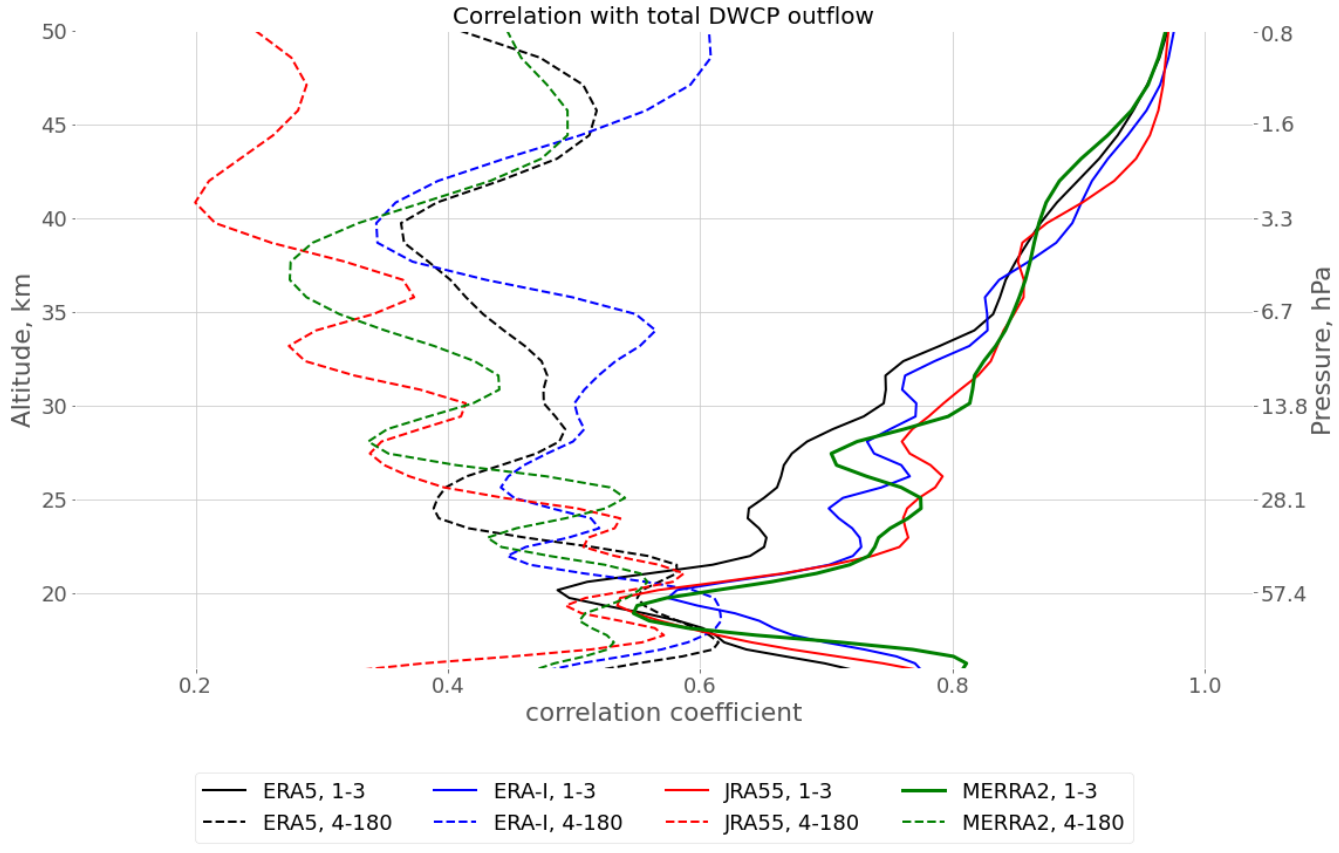

Figure 7. Vertical profile of the correlation coefficients between total outflow driven by all waves and the outflow driven by only large-scale planetary (solid) and smaller-scale waves (dashed). Profiles have been constructed from 1980-2017 monthly mean data. The lines were smoothed with a Gaussian filter.

https://doi.org/10.5194/egusphere-2024-4088
Preprint. Discussion started: 21 January 2025

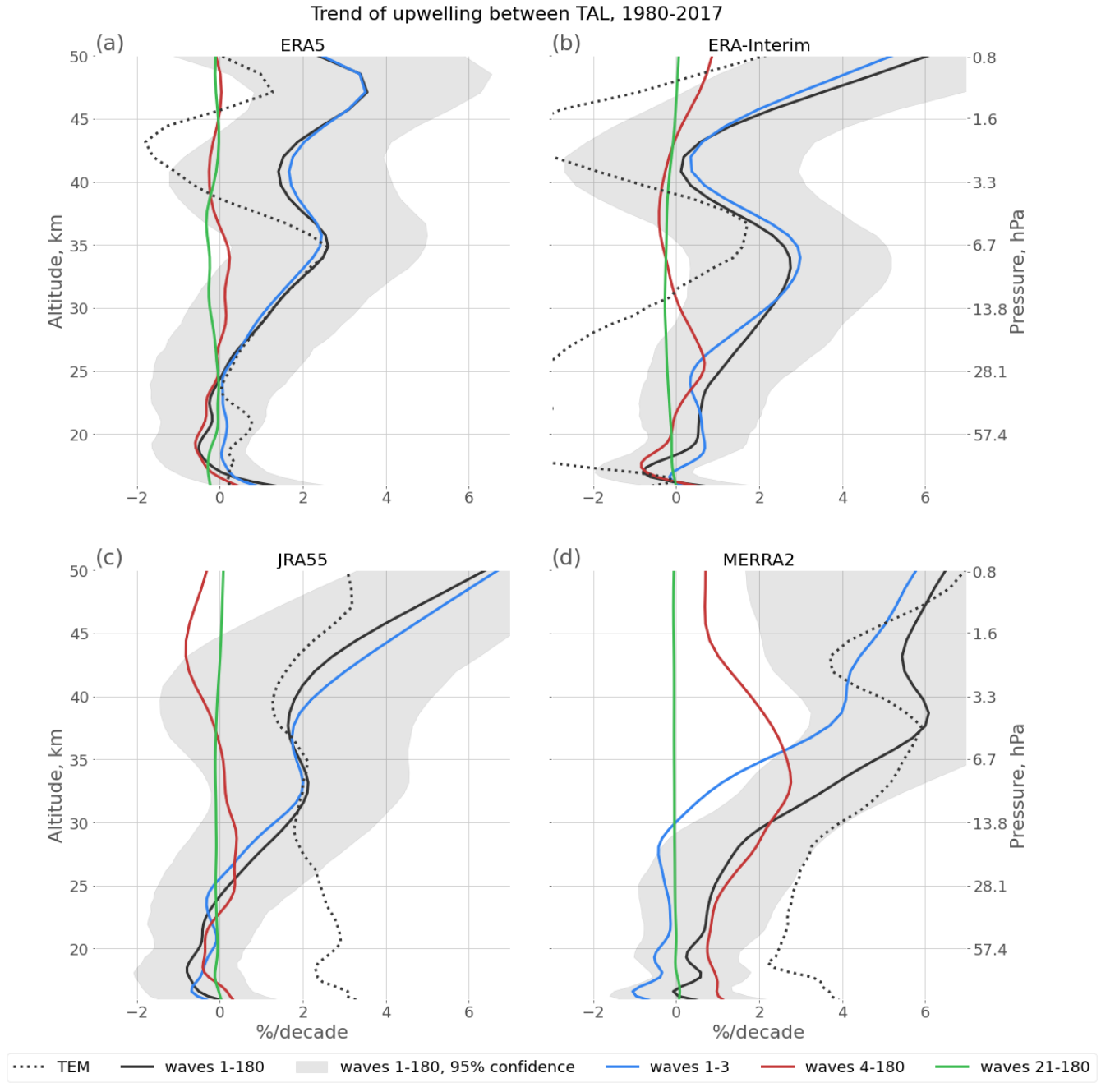

Figure 8. Vertical profiles of upwelling trend derived using TEM (dotted black line) or DWCP from total (black), large-scale planetary (blue), smaller-scale (red), and gravity (green) waves, gray shading denotes 95 percent confidence interval for total waves. The profiles were constructed from annual mean data ERA5 (a), ERA-Interim (b), JRA55 (c), and MERRA2 (d). The lines were smoothed with Gaussian filter.

https://doi.org/10.5194/egusphere-2024-4088
Preprint. Discussion started: 21 January 2025

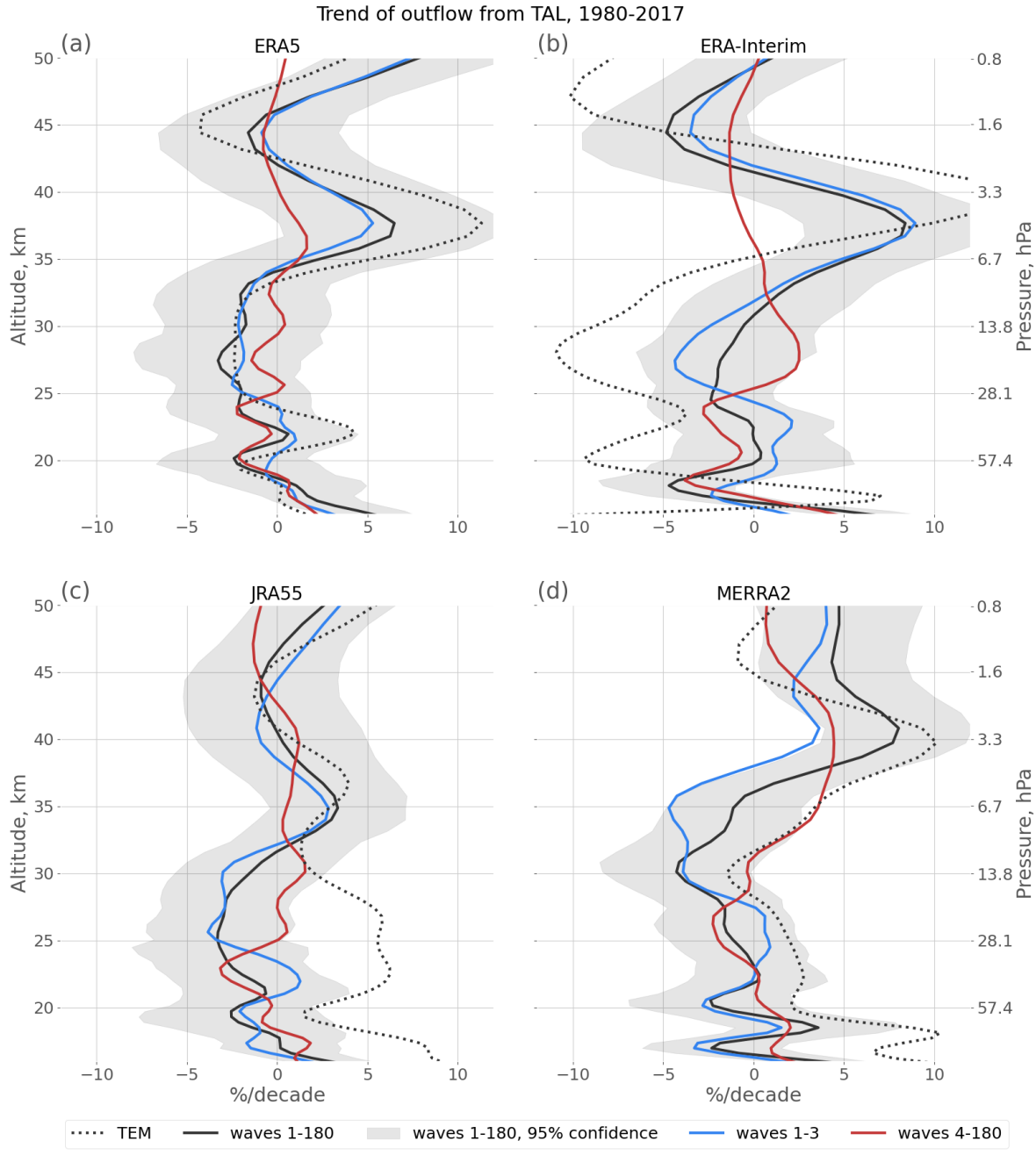

Figure 9. Vertical profiles of outflow trend derived using TEM (dotted black line) or DC from total (black), large-scale planetary (blue), and smaller-scale(red) waves, gray shading denotes 95 percent confidence interval for total waves. The profiles were constructed from annual mean data ERA5 (a), ERA-Interim (b), JRA55 (c), and MERRA2 (d). The lines were smoothed with Gaussian filter.

https://doi.org/10.5194/egusphere-2024-4088
Preprint. Discussion started: 21 January 2025

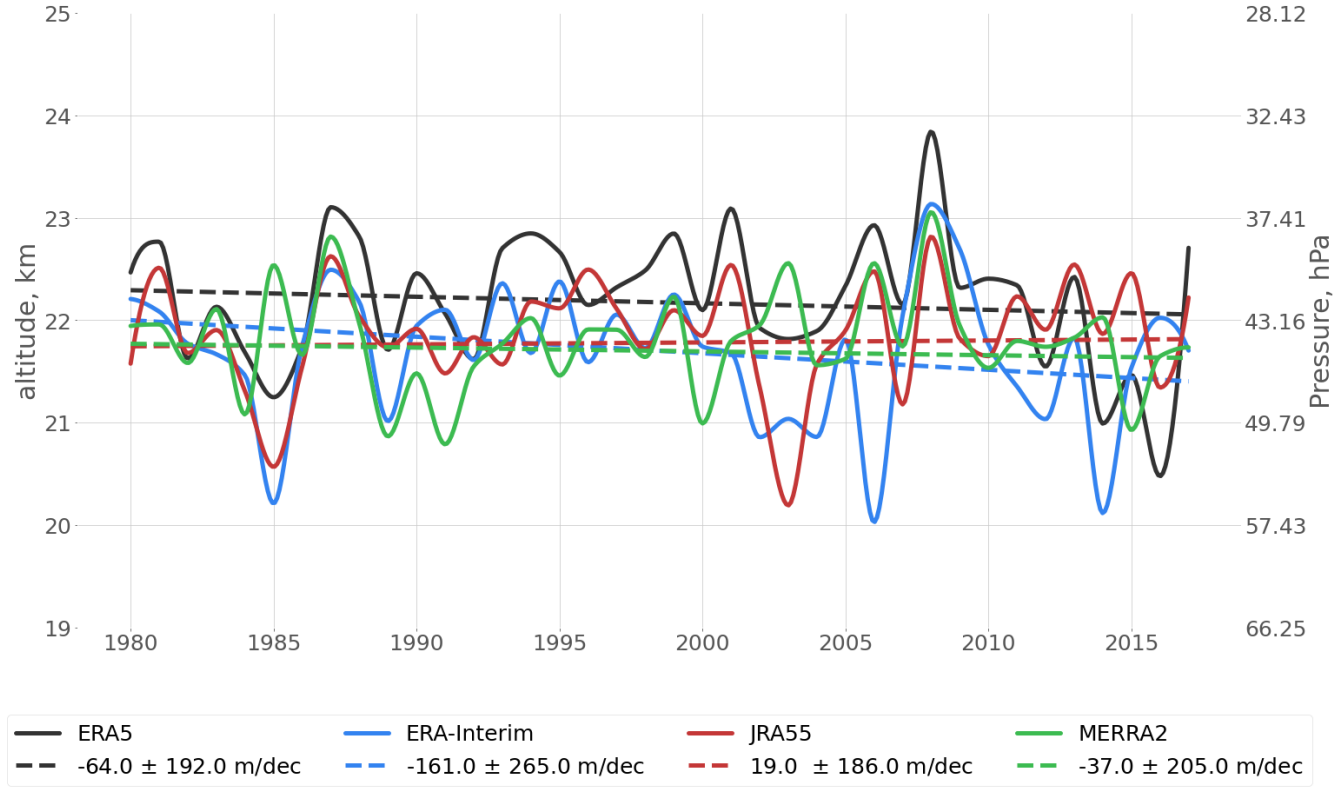

Figure 10. The variability and trend of the separation level between shallow and deep stratospheric circulation branches over the period 1980-2017 from ERA5 (black), ERA-Interim (blue), JRA55 (red), and MERRA2 (green). Solid lines represent the annual mean separation level and dashed lines show the linear trend based on the annual mean level. Decadal trend values ±2 standard error are given in the legend.

https://doi.org/10.5194/egusphere-2024-4088
Preprint. Discussion started: 21 January 2025

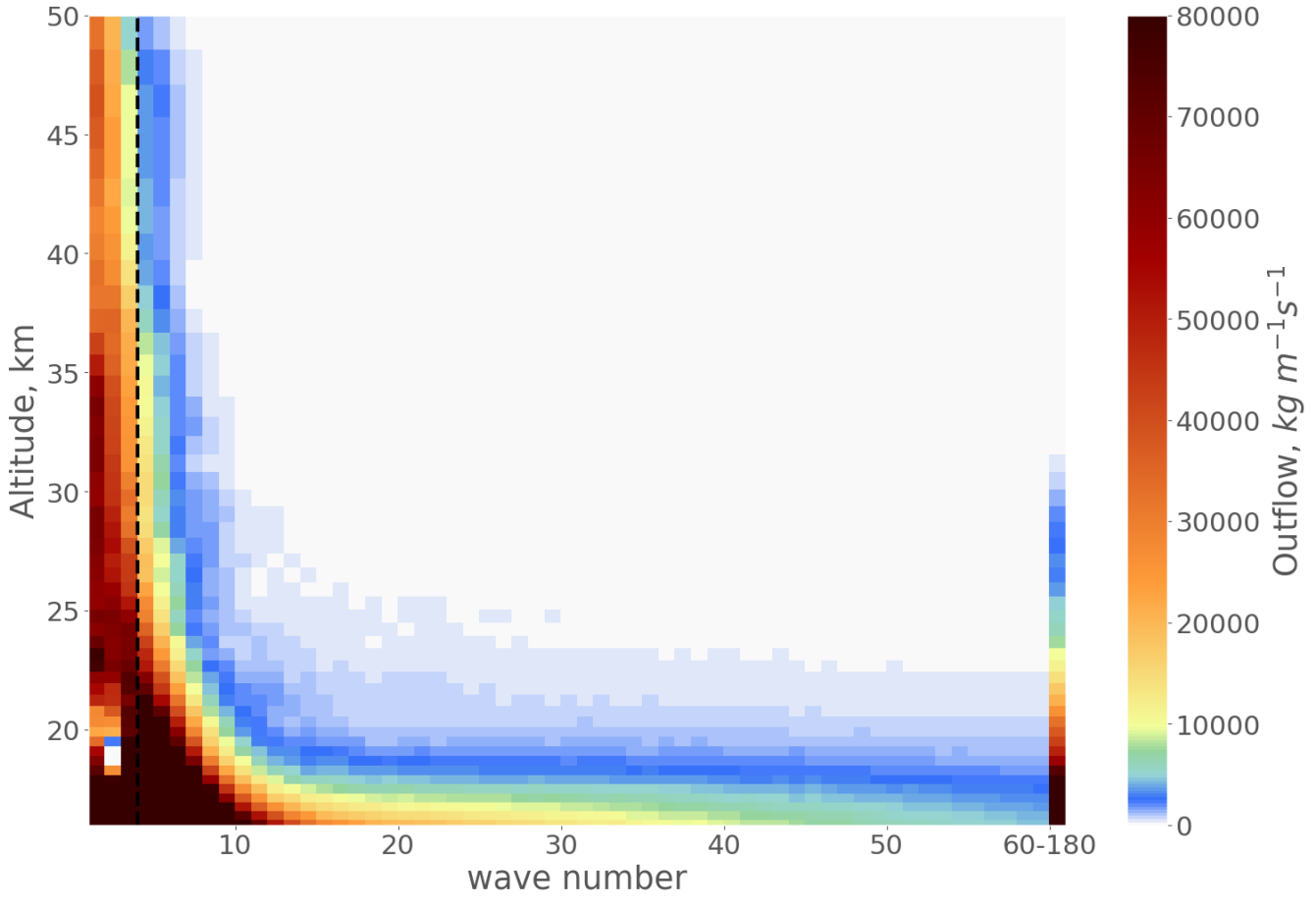

Figure A1. 1980-2017 mean vertical profiles of outflow estimated for different waves from EPF divergence calculations based on ERA5 data using the downward control principle.

https://doi.org/10.5194/egusphere-2024-4088
Preprint. Discussion started: 21 January 2025

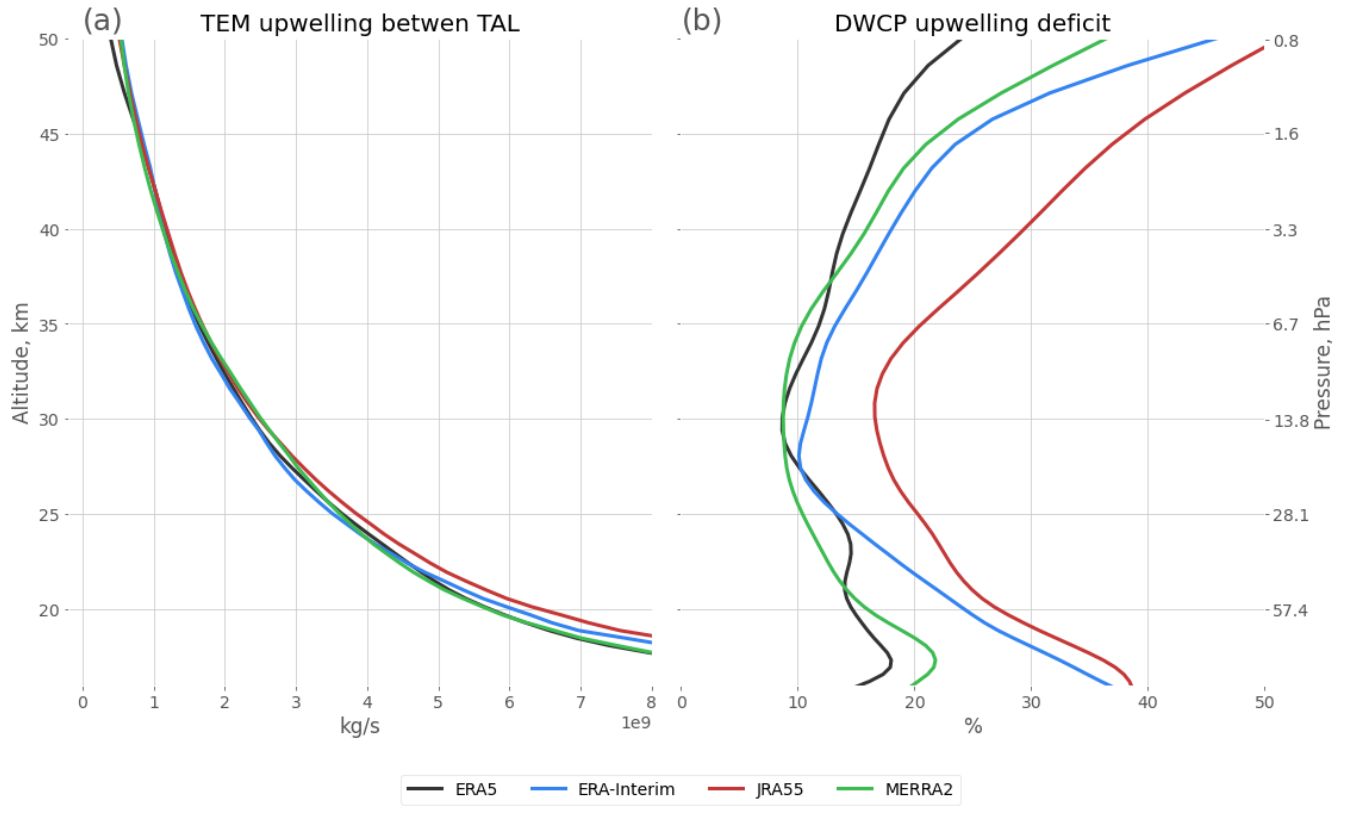

Figure A2. (a) 1980-2017 mean profiles of TEM upwelling from ERA5 (black), Era-Interim (blue), JRA55 (red), and MERRA2 (green) reanalyses. (b) The mean upwelling deficit in the downward control calculation (in percent), estimated as the relative difference between TEM and downward control upwelling. This upwelling deficit corresponds to the missing wave drag in the downward calculation (see text). The deficit lines were smoothed with a Gaussian filter. The black line for ERA5 upwelling in (a) in the lower stratosphere mostly overlaps with the green MERRA2 line.

https://doi.org/10.5194/egusphere-2024-4088
Preprint. Discussion started: 21 January 2025

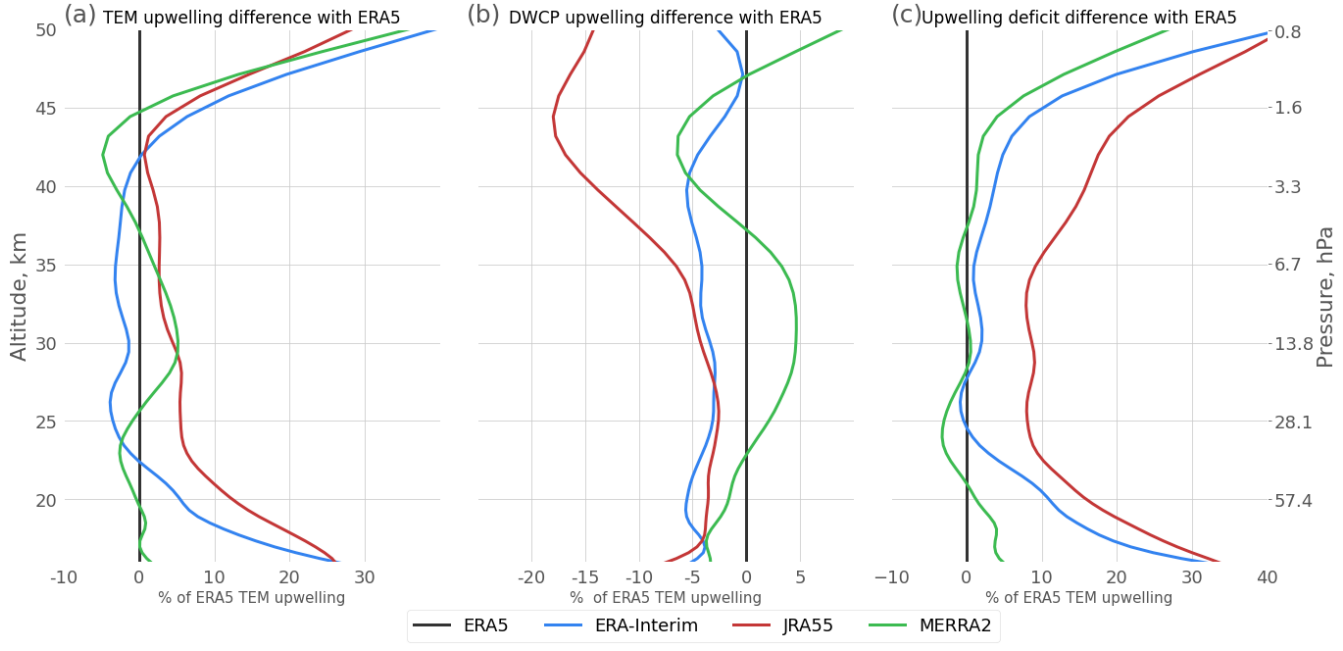

Figure A3. Reanalyses upwelling inter-comparison with ERA5 as base, for TEM upwelling (a), DWCP upwelling (b), and upwelling deficit (c)

https://doi.org/10.5194/egusphere-2024-4088
Preprint. Discussion started: 21 January 2025

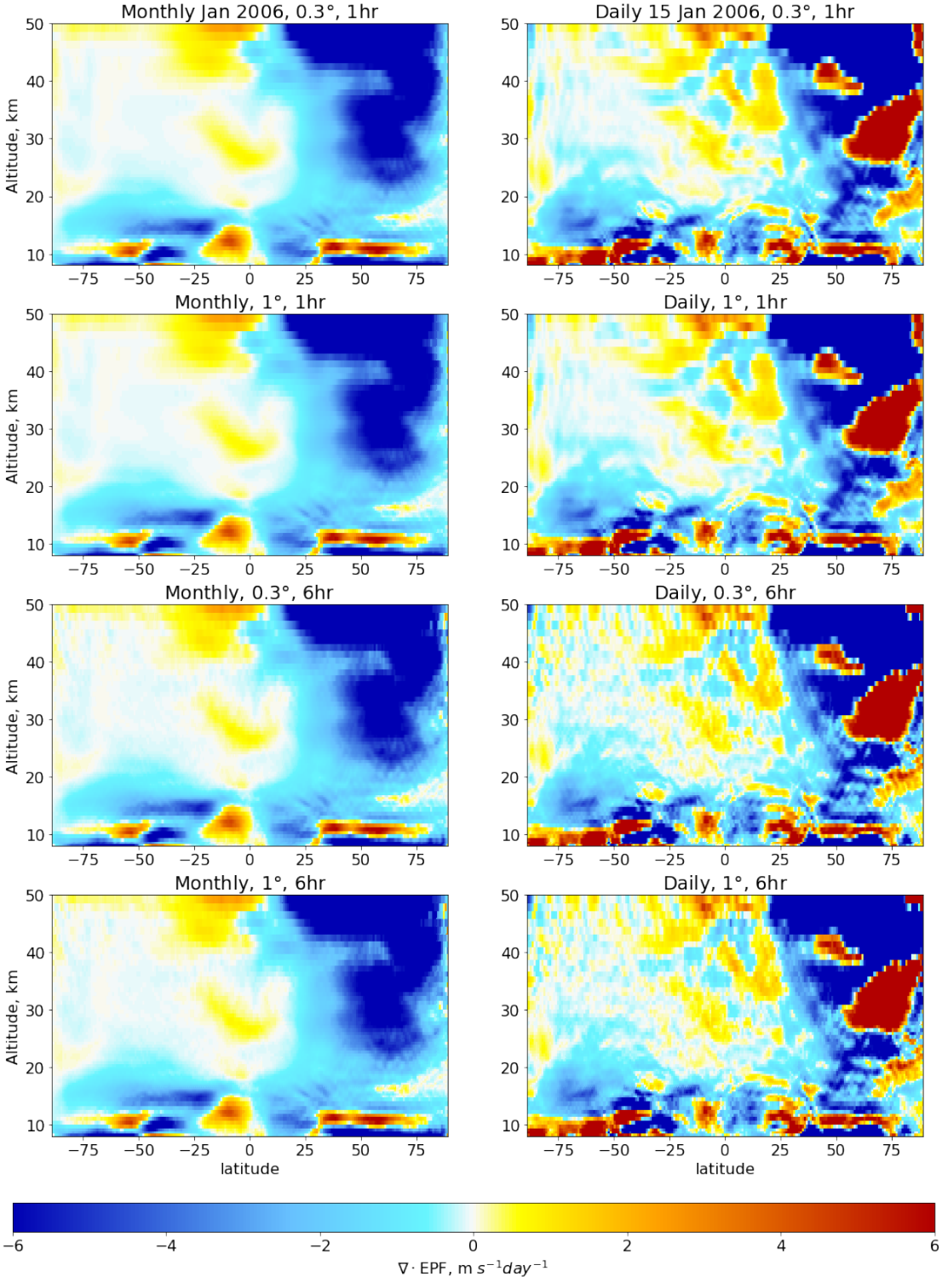

Figure A4. Effect of reduction of spatial (from 0.3° to 1°) and temporal (from 1 to 6 hours) resolution on ∇·EPF calculations

https://doi.org/10.5194/egusphere-2024-4088
Preprint. Discussion started: 21 January 2025

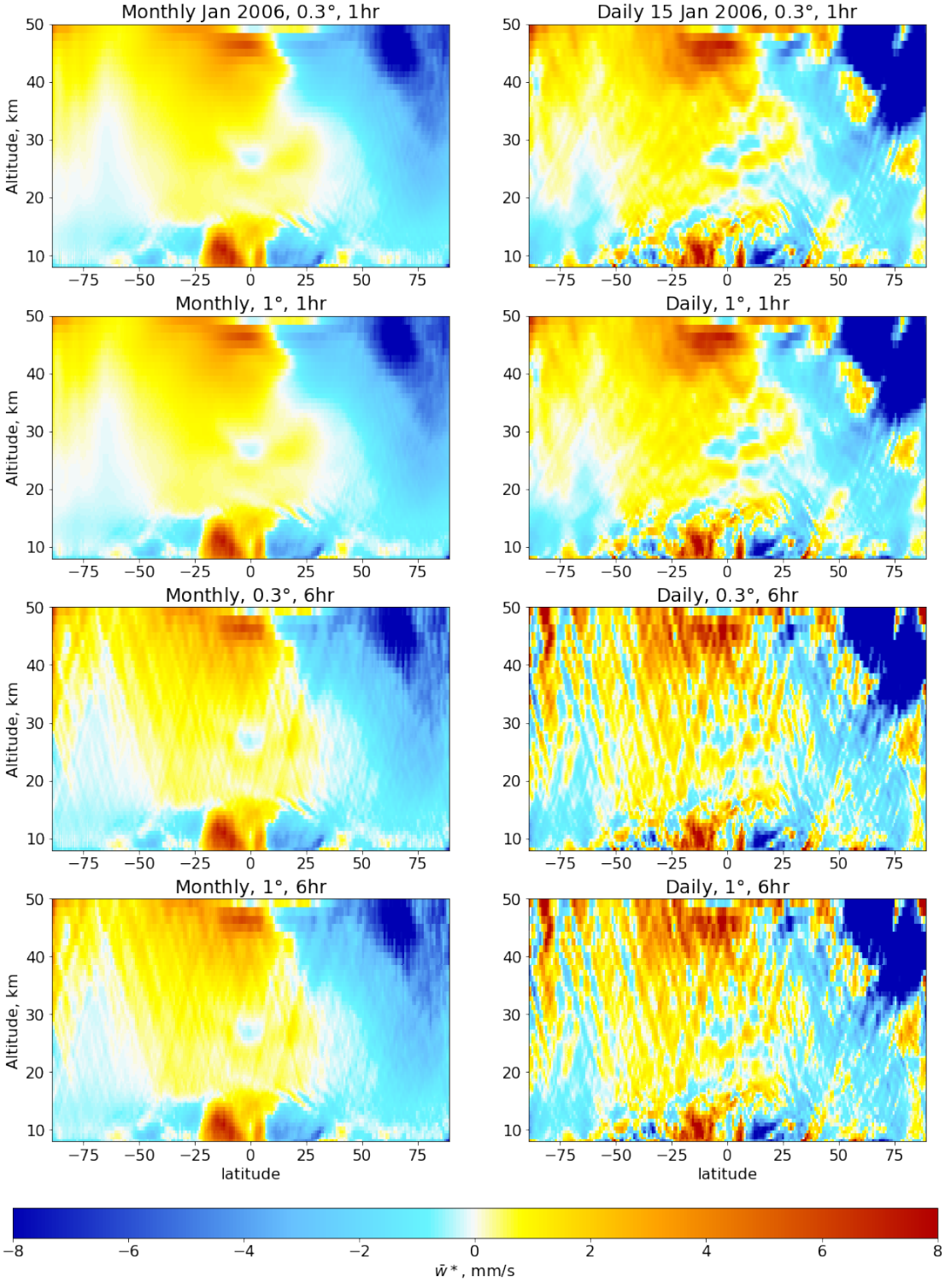

Figure A5. Effect of reduction of spatial (from 0.3° to 1°) and temporal (from 1 to 6 hours) resolution on $\bar{w}^*$ calculations